https://doi.org/10.5194/egusphere-2026-6595
Preprint. Discussion started: 10 November 2026
© Author(s) 2026. CC BY 4.0 License.

Wintertime VOC distributions, emission signatures, and transboundary transport over the Seoul Metropolitan Area and the Yellow Sea from airborne observations during ASIA-AQ

Jimin Lee[1], Jinsoo Park[2], Jeongho Kim[3], Limseok Chang[2], Jinsoo Choi[2], Minyoung Sung[2], Gangwoong Lee[4], Jeonghwan Kim[4], Jongho Kim[5], Eric C. Apel[6], Rebecca S. Hornbrook[6], Donald R. Blake[7], Isobel J. Simpson[7], Armin Wisthaler[8,9], Wojciech Wojnowski[8,10], Felix Piel[8,a], Glenn S. Diskin[11], Jason A. Miech[11,12], Joshua P. DiGangi[11], Yonghoon Choi[11,12], Alessandro Franchin[6], Changmin Cho[6], Saewung Kim[13], Meehye Lee[1,*]

[1] Department of Earth and Environmental Sciences, Korea University, Seoul, South Korea
[2] Environmental Satellite Center, National Institute of Environmental Research, Incheon, South Korea
[3] Open Space Co., Seoul, South Korea
[4] Department of Environmental Science, Hankuk University of Foreign Studies, Yongin, South Korea
[5] Environmental Research Center, Hanseo University, Seosan, South Korea
[6] Atmospheric Chemistry Observations & Modeling Laboratory, U.S. National Science Foundation National Center for Atmospheric Research, Boulder, CO, USA
[7] Department of Chemistry, University of California, Irvine, CA, USA
[8] Department of Chemistry, University of Oslo, Oslo, Norway
[9] Institute for Ion Physics and Applied Physics, University of Innsbruck, Innsbruck, Austria
[10] Department of Analytical Chemistry, Gdańsk University of Technology, Gdańsk, Poland
[11] NASA Langley Research Center, Hampton, VA, USA
[12] Analytical Mechanics Associates, Hampton, VA, USA
[13] Department of Earth Science, University of California, Irvine, CA, USA
[a] now at: Advanced Monitoring Solutions (adMS), Oslo, Norway

Correspondence to: Meehye Lee (meehye@korea.ac.kr)

https://doi.org/10.5194/egusphere-2026-6595
Preprint. Discussion started: 10 November 2026
© Author(s) 2026. CC BY 4.0 License.



Abstract. Volatile organic compounds (VOCs) are key precursors of ozone and secondary organic aerosol, yet wintertime constraints on how local emissions, chemical lifetime, and regional transport jointly shape VOC distributions over Korea and the Yellow Sea remain limited based on airborne measurements. We analyzed proton-transfer-reaction time-of-flight mass spectrometry (PTR-ToF-MS) measurements from 17 Beechcraft 1900D flights during the 2024 Airborne and Satellite Investigation of Asian Air Quality (ASIA-AQ) campaign. The sum of seven VOC species or groups was 2.4 times higher over Seoul than over the Yellow Sea. Toluene, C_8 aromatics, and a methyl ethyl ketone (MEK)-equivalent signal were strongly enhanced in low-altitude, source-influenced air masses, whereas benzene, acetone, and acetonitrile showed weaker regional and vertical contrasts. Seoul-to-Yellow Sea VOC-to-benzene slope ratios generally increased with chemical reactivity, but toluene and C_8 aromatics showed positive deviations, indicating an additional influence of urban aromatic source composition. Yellow Sea observations, supported by NASA DC-8 measurements, indicated continental outflow. An order-of-magnitude transport analysis estimated distance scaled Yellow Sea transport equivalents of approximately 30 % of Seoul benzene emissions in the Clean Air Policy Support System inventory and 6 % for toluene. Wintertime VOC variability is thus species dependent: urban and industrial emissions dominate reactive aromatic VOCs, whereas longer-lived benzene is more sensitive to regional transport. Effective wintertime VOC management requires species-specific strategies considering domestic emissions and regional inflow.

https://doi.org/10.5194/egusphere-2026-6595
Preprint. Discussion started: 10 November 2026
© Author(s) 2026. CC BY 4.0 License.

1 Introduction

Volatile organic compounds (VOCs) play a pivotal role in atmospheric chemistry and directly affect air quality at both regional and global scales. VOCs react with atmospheric oxidants, including OH, ozone (O_3), and NO_3, and participate in photochemical reaction sequences that produce O_3 and secondary organic aerosol (SOA) (Atkinson, 2000; Kleindienst et al., 1999; Seinfeld and Pandis, 2016). Through their roles as precursors of O_3 and SOA, VOCs influence climate-relevant atmospheric composition as well as regional air quality. Some VOCs, such as benzene, also pose significant health hazards and require continuous management through regulated environmental standards. VOCs therefore provide a critical link between primary emissions, secondary pollutant formation, climate-relevant atmospheric composition, and human exposure.

However, understanding the behavior of VOCs remains challenging because their emission sources, atmospheric lifetimes, oxidation mechanisms, and product yields vary widely depending on the photochemical environment and meteorological conditions. VOCs are emitted from diverse anthropogenic sources, including automobiles, industrial activities, solvent use, combustion processes, and gasoline evaporation, as well as from biogenic sources such as vegetation and wildfires (Cetin et al., 2003; Derwent et al., 2000; Gilman et al., 2015; Guenther et al., 2013; Guo et al., 2006). Secondary formation can also contribute to atmospheric levels, particularly for oxygenated VOCs such as acetone and methyl ethyl ketone (MEK), which can be produced during the atmospheric oxidation of precursor hydrocarbons (Singh et al., 2004). Many VOCs are highly reactive, and their oxidation involves highly nonlinear chemistry due to feedback between radicals (Atkinson, 2000). Highly reactive VOCs can be removed within minutes and affect air quality in local areas, but less reactive compounds with longer lifetimes can persist in the atmosphere for days to weeks and influence air quality in distant regions through long-range atmospheric transport (Atkinson, 1997; Ryerson et al., 2003). Therefore, species-resolved VOC measurements are essential for understanding photochemical pollution mechanisms and developing effective control strategies for air quality and climate change.

In Northeast Asia, prevailing westerlies frequently carry anthropogenic pollutants from the Asian continent across the Yellow Sea toward the North Pacific Ocean (Griffith et al., 2020; Huebert et al., 2003; Itahashi et al., 2017). Located between major continental source regions in eastern China and receptor regions such as the Korean Peninsula and Japan, the Yellow Sea is therefore a key transport corridor and receptor region where VOC composition can reflect both continental outflow and chemical aging before air masses reach the Korean Peninsula (Choi et al., 2019; Kim et al., 2018; Lee et al., 2015; Park et al., 2024; Wang et al., 2023).

In South Korea, airborne measurement-based air quality observation campaigns, such as the Megacity Air Pollution Study (MAPS-Seoul) in 2015 and the Korea-United States Air Quality (KORUS-AQ) campaign in 2016, have provided opportunities to collect high-resolution air quality observational data (Crawford et al., 2021; Kim et al., 2018). Specifically, MAPS-Seoul and KORUS-AQ provided high-resolution observational constraints on domestic emissions and secondary pollutant formation during May–June, when photochemistry is active (Fried et al., 2020; Kwon et al., 2021; Nault et al., 2018; Simpson et al., 2020). Much less is known, however, about how wintertime boundary layer structure, reduced photochemical loss, and synoptic transport shape VOC distributions over Korea and the Yellow Sea.

The Airborne and Satellite Investigation of Asian Air Quality (ASIA-AQ) campaign was designed to enhance understanding of sources, chemical transformations, and regional transport of air pollutants across Asia, and its

https://doi.org/10.5194/egusphere-2026-6595
Preprint. Discussion started: 10 November 2026
© Author(s) 2026. CC BY 4.0 License.

VOC measurements serve as a key element in linking primary emissions to the formation of secondary pollutants (Crawford et al., 2022). Airborne observations also provide unique and indispensable information on the vertical distribution of atmospheric species (Hudman et al., 2009; Li et al., 2016; Mazzuca et al., 2016; Ryerson et al., 2013), enabling improved assessment of emission strengths, transport processes, and photochemical evolution within the boundary layer and free troposphere (Caicedo et al., 2019; Chen et al., 2019; Jin et al., 2023; Mazzuca et al., 2016; Travis et al., 2020). However, airborne observations of VOC concentrations and their vertical distributions in both the free troposphere and planetary boundary layer (PBL) over Korea and the Yellow Sea remain very limited (Wang et al., 2023; Wu et al., 2021). The 1900D platform provided repeated low-altitude sampling within the PBL over Seoul and adjacent coastal industrial regions, complementing the broader regional and vertical coverage of the NASA DC-8.

Here we use 1900D airborne PTR-ToF-MS observations from the ASIA-AQ campaign to characterize wintertime VOC distributions over the Seoul Metropolitan Area (SMA), adjacent western coastal industrial regions, and the Yellow Sea. The central objective is to examine how chemical lifetime, emission source specificity, and regional transport jointly shape wintertime VOC variability over the SMA and the Yellow Sea. We first characterize three-dimensional distributions of key VOC groups, then use inter-species relationships and benzene-normalized slopes to distinguish local source signatures from regionally transported signals. Finally, we compare selected observations with the Clean Air Policy Support System (CAPSS) emission inventory (Choi et al., 2022; Lee et al., 2024) and provide an order-of-magnitude estimate of eastward benzene and toluene transport across the Yellow Sea.

2 Methods

2.1 Airborne measurements during the ASIA-AQ campaign

Airborne observations were conducted aboard a Beechcraft 1900D aircraft operated by Hanseo University and the National Institute of Environmental Research (NIER) during the South Korea deployment of the ASIA-AQ campaign. During the South Korea deployment, the 1900D research flights were operated from Osan Air Base, Republic of Korea. A proton transfer reaction time-of-flight mass spectrometer (PTR-ToF-MS 1000, Ionicon, Austria) was installed onboard to measure VOCs in real time. Seventeen flights were conducted from 6 February to 10 March 2024.

The flight domain included the SMA, adjacent western coastal industrial regions, and the Yellow Sea. Four flights focused primarily on the SMA, one flight targeted the Yellow Sea, and the remaining twelve flights included repeated low-altitude transects over densely populated and source-influenced areas, while also sampling marine air masses and regional transport pathways over the Yellow Sea (Fig. 1).

The metropolitan flight patterns were designed to span altitudes from approximately 200 m to 3000 m, allowing VOC distributions to be examined across the PBL and lower free troposphere. These flights also provided an opportunity to directly sample source-influenced air masses within the PBL over Seoul and nearby industrial regions. In addition, a repeated low-altitude flight leg over the Yellow Sea was conducted at approximately 250 m along 124° E to characterize near-surface VOC distributions over the marine transport corridor.

https://doi.org/10.5194/egusphere-2026-6595
Preprint. Discussion started: 10 November 2026
© Author(s) 2026. CC BY 4.0 License.

The flight tracks passed over or near several major emission regions, including central Seoul, Bucheon, the Ansan–Sihwa industrial complex, and the western coastal corridor toward Daesan. The Ansan–Sihwa (Banwol–Sihwa) industrial complex, located southwest of Seoul, is one of the largest industrial areas in South Korea and includes petrochemical production, metal-processing, rubber, plastic, and other manufacturing activities (Kim et al., 2020; Park et al., 2001, 2016). The southwestern flight track also includes regions potentially influenced by emissions from the Daesan petrochemical complex in South Chungcheong Province (Baek et al., 2020). These flight patterns therefore enabled comparison between urban source regions, coastal industrial plumes, and air masses transported over the Yellow Sea.

https://doi.org/10.5194/egusphere-2026-6595
Preprint. Discussion started: 10 November 2026
© Author(s) 2026. CC BY 4.0 License.

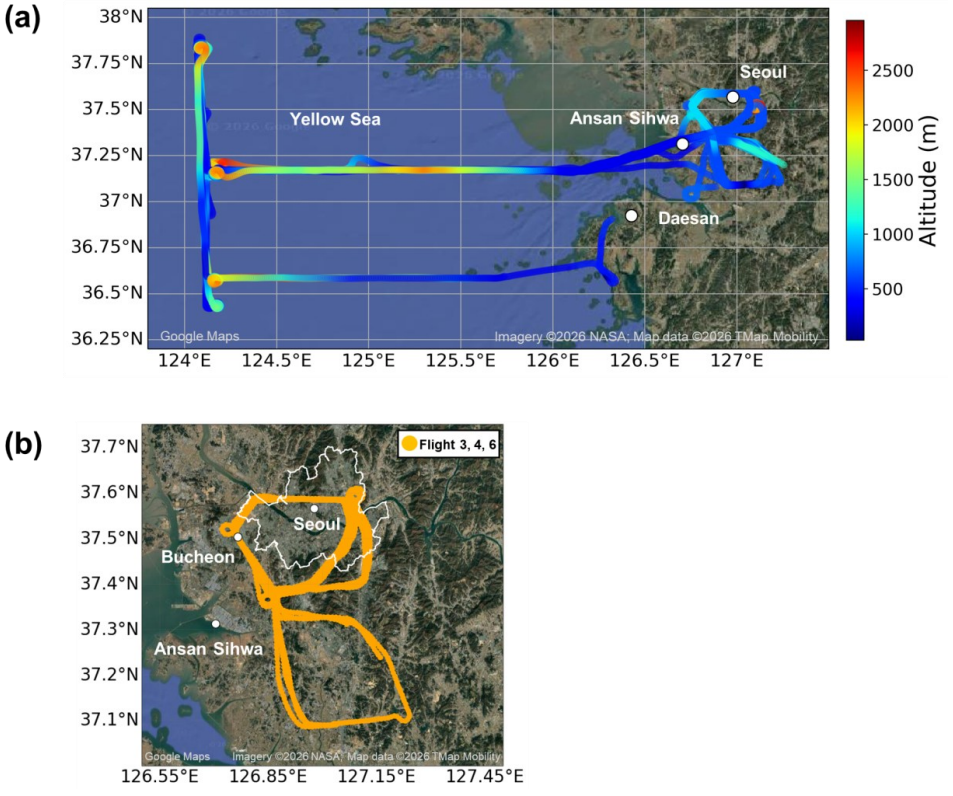


Figure 1: Flight tracks of the 1900D aircraft during ASIA-AQ. (a) Flight tracks are colored by altitude (m), showing flight paths over the Yellow Sea, Ansan–Sihwa industrial complex, Daesan industrial area, and Seoul Metropolitan Area. (b) Selected flights (Flights 3, 4, and 6) over Seoul and the surrounding metropolitan area, with white lines indicating the administrative boundary of Seoul.

https://doi.org/10.5194/egusphere-2026-6595
Preprint. Discussion started: 10 November 2026
© Author(s) 2026. CC BY 4.0 License.

2.2 VOC measurements using PTR-ToF-MS aboard the 1900D

Volatile organic compounds were measured in real time using a proton-transfer-reaction time-of-flight mass spectrometer (PTR-ToF-MS 1000, Ionicon Analytik, Austria) installed onboard the Beechcraft 1900D aircraft. Ambient air was drawn through a 1/4-inch Teflon inlet mounted on the left-front side of the aircraft at a total flow rate of 5 L min^{-1} using a mass-flow-controlled sampling line. A subsequent flow of 100 mL min^{-1} was introduced into the PTR-ToF-MS through an 8-port sample switching valve and 1/16-inch PEEK tubing heated to 60 °C. The estimated transit time from the inlet to the detector was approximately 0.6 s, allowing high temporal resolution airborne measurements during flight. The PTR-ToF-MS operated with H_3O^+ chemical ionization. VOCs with a proton affinity higher than that of water were ionized through proton transfer reactions to form protonated product ions (Blake et al., 2009; de Gouw and Warneke, 2007; Hewitt et al., 2003). The drift tube was maintained at 600 V DC (direct current), 80 °C, and 2.4 mbar, corresponding to a reduced electric field (E/N, the ratio of the electric field E to the buffer gas number density N) of 140 Td (Townsend, 1 Td = 10^{-17} V cm^2). Ions were detected over the m/z 10–500 range, with ion extraction at 35 kHz, and mass spectra were acquired at 1 s time resolution (Table 1; Müller et al., 2014; Piel et al., 2019).

The analysis focused on seven target VOC species or groups: benzene (m/z 79.054), toluene (m/z 93.070), C_8 aromatics reported as the unresolved sum of xylenes and ethylbenzene (m/z 107.086), trimethylbenzenes (m/z 121.101), MEK-equivalent signal (m/z 73.065), acetonitrile (m/z 42.034), and acetone (m/z 59.049). Because the PTR-ToF-MS does not separate structural isomers at a given nominal mass, the C_8 aromatic signal is interpreted as a combined xylene/ethylbenzene group, and the trimethylbenzene signal represents unresolved trimethylbenzene isomers. The m/z 73.065 signal is reported as MEK-equivalent because possible isobaric oxygenated VOC contributions cannot be fully excluded. Trimethylbenzenes were not directly calibrated, and their sensitivity was estimated from the mass-transmission relationship, resulting in greater uncertainty than for the directly calibrated species.

Calibration was performed using oxygenated VOC and TO-14 standard gas mixtures. Mass-dependent transmission efficiency was determined by introducing standard gas at known concentrations and comparing ion signal intensities as a function of m/z. A mass-transmission curve was generated using a mixed VOC standard gas at approximately 100 ppbv, and species sensitivities were calculated in counts per second per ppbv (cps $ppbv^{-1}$). Multiple-point calibrations were conducted over a 0–46 ppbv range, and most directly calibrated compounds showed coefficients of determination (r^2) greater than 0.98.

Calibration and sensitivity checks were conducted before and after research flights to evaluate instrumental stability. Background signals were determined from zero-air measurements during the calibration sequence, and the corresponding background corrections and calibration factors were applied during spectral processing. VOC concentrations were calculated using PTR-ToF-MS Viewer v3.4, including nonlinearity correction of ion count rates, mass-axis calibration, peak fitting where applicable, background subtraction, and mass-transmission correction.

Raw mass spectra were acquired at 1-s resolution. For the analysis presented here, a 10-s rolling mean was applied to improve the signal-to-noise ratio. Detection limits for the 10-s averaged data ranged from 0.02 to 0.10 ppbv (Table S1). The 1-s raw data correspond to an along-track distance of approximately 70–100 m, depending on

https://doi.org/10.5194/egusphere-2026-6595
Preprint. Discussion started: 10 November 2026
© Author(s) 2026. CC BY 4.0 License.

aircraft speed, whereas the smoothed data represent an effective horizontal smoothing scale of approximately 0.7–1.0 km. The overall uncertainty for directly calibrated species was 8.5–12 %, with larger uncertainty expected for the trimethylbenzenes, because their sensitivity was estimated from the mass-transmission curve rather than direct calibration.

Table 1: Operating conditions of the PTR-ToF-MS.

Component	Parameter	Analytical condition
Ion drift tube	Drift tube temperature	80 °C
	Drift voltage	600 V DC
	Reduced electric field (E/N)	140 Td
	Drift tube pressure	2.4 mbar
Time-of-flight mass analyzer	Mass range	m/z 10–500
	Ion extraction rate	35 kHz
	Acquisition interval	1 s

2.3 Meteorological measurements and PBL classification

Meteorological parameters were measured in real time using the Aircraft Integrated Meteorological Measurement System (AIMMS-30; Aventech Research, Inc., Canada) installed aboard the 1900D aircraft. The system provided three-dimensional position, aircraft velocity and attitude, wind components, temperature, relative humidity, and pressure at 1-Hz resolution. Aircraft position and motion were determined using the integrated GPS receivers and a six-degree-of-freedom inertial measurement unit. Static and dynamic pressure, ambient temperature, and relative humidity were measured with a five-hole air data probe mounted on the aircraft fuselage. The AIMMS-30 data were processed using the internal Kalman filter-based fusion algorithm. The reported measurement accuracies were better than 0.25° for aircraft attitude, ± 0.5 m s^{-1} for horizontal and vertical wind components, ± 0.3 °C for temperature, and ± 2 % for relative humidity. Temperature, relative humidity, and pressure were recorded at resolutions of 0.01 °C, 0.05 %, and 0.1 hPa, respectively (Kim et al., 2025). Calibration coefficients obtained from dedicated aircraft calibration maneuvers were applied during post-processing to improve wind and airflow measurements. The processed meteorological data were used to characterize vertical structure and wind conditions and to support PBL classification and advective transport analyses during the campaign.

Planetary boundary layer height (PBLH) was estimated from aircraft vertical profiles using combined gradients in VOC mixing ratios, potential temperature, and relative humidity. For each available ascent and descent profile, transition altitudes were identified from coincident changes in VOC vertical gradients and thermodynamic variables. The VOC-gradient method identifies altitudes where the vertical gradient changes sharply, whereas the thermodynamic method identifies layers where potential temperature increases and relative humidity decreases

https://doi.org/10.5194/egusphere-2026-6595
Preprint. Discussion started: 10 November 2026
© Author(s) 2026. CC BY 4.0 License.



across the transition from the mixed layer to the lower free troposphere. This combined approach is consistent with previous profile-based and aircraft-supported PBLH determinations (Berkes et al., 2016; Sasakawa et al., 2013; Seidel et al., 2010).

The three diagnostics generally converged near 1100 m during representative vertical profiles, with differences within approximately ± 100 m. We therefore used 1100 m as an operational threshold to classify observations as within or above the PBL in campaign-scale analyses. Because PBLH varies among flights and evolves diurnally, this fixed threshold should be interpreted as a practical classification criterion rather than as a fully flight-resolved mixed-layer height. Results that depend directly on this threshold, particularly PBL-integrated flux estimates, were therefore evaluated with sensitivity to the assumed PBL depth where relevant.

2.4 Ground-based VOC measurements

Ground-based VOC measurements were conducted at the Mediheal EES Hall of Korea University (37.585° N, 127.026° E) in Seongbuk-gu, Seoul, from 25 January to 25 March 2024. The site is located in a mixed residential and commercial area in northeastern Seoul and served as one of the Seoul ground observation sites during ASIA-AQ. For comparison with the 1900D observations, measurements from 6 February to 10 March 2024, corresponding to the 1900D campaign period, were used.

Aromatic hydrocarbons used in this study were measured using an online thermal desorption gas chromatography–flame ionization detection system (TD-GC-FID; UNITY-xr, Markes International, UK; 8890 GC, Agilent Technologies, USA). Ambient air was collected onto adsorbent tubes at 15 mL min^{-1} for 40 min and analyzed after thermal desorption and chromatographic separation. Mixing ratios were quantified using multipoint external calibration with certified Photochemical Assessment Monitoring Stations (PAMS) VOC standard gas mixtures. Routine QA/QC included multipoint calibration, blank analysis, cold-trap performance checks, retention-time checks, and periodic instrument performance verification. Acetone, MEK, and acetonitrile were measured in real time using a ground-based PTR-ToF-MS (Ionicon Analytik GmbH, Austria) operated with H_3O^+ reagent ions at an E/N of 120 Td. Instrument sensitivities were determined using multipoint calibrations with certified standard gas mixtures, and instrument performance was routinely evaluated using standard gas and zero-air measurements. For the ground-to-aircraft comparison, C_8 aromatics, toluene, benzene, and trimethylbenzenes were obtained from the TD-GC-FID measurements, whereas MEK, acetonitrile, and acetone were obtained from the PTR-ToF-MS measurements.

3 Results and discussion

3.1 Measurement overview

Seventeen 1900D flights sampled the Seoul Metropolitan Area (SMA), Gyeonggi Province, including the western coastal industrial corridor, and the Yellow Sea (YS) during February–March 2024 (Table 2). The sum of the seven target VOC mixing ratios is denoted as Σ_7VOCs. Across all flights, mean Σ_7VOCs was 2.38 ± 1.39 ppbv. Acetone showed the highest mean mixing ratio of 0.86 ± 0.31 ppbv, followed by MEK-equivalent signal (0.50 ± 0.38

https://doi.org/10.5194/egusphere-2026-6595
Preprint. Discussion started: 10 November 2026
© Author(s) 2026. CC BY 4.0 License.

ppbv), toluene (0.44 ± 0.49 ppbv), benzene (0.20 ± 0.08 ppbv), trimethylbenzenes (0.19 ± 0.09 ppbv), C_8 aromatics (0.12 ± 0.11 ppbv), and acetonitrile (0.09 ± 0.02 ppbv). Acetone accounted for 36 % of Σ_7VOCs, whereas MEK-equivalent signal, toluene, and benzene contributed 21 %, 18 %, and 8 %, respectively.

The highest mean Σ_7VOCs values were observed during the SMA-focused flights. Flight 3, conducted over Seoul and the surrounding metropolitan region, showed the highest Σ_7VOCs value of 6.12 ± 1.67 ppbv. During this flight, toluene reached a mean concentration of 1.92 ± 1.08 ppbv, the highest among all flights. Flight 6, also conducted over the SMA but during the afternoon, showed the second-highest Σ_7VOCs value of 5.10 ± 1.02 ppbv and the highest MEK-equivalent concentration of 1.41 ± 0.65 ppbv. Flight 4 showed the third-highest Σ_7VOCs value (3.77 ± 1.40 ppbv), with acetone, MEK-equivalent signal, and toluene together accounting for most of the measured Σ_7VOCs. In contrast, Flight 1 ended approximately one hour after takeoff and did not complete the planned SMA observation; it showed the lowest flight-mean Σ_7VOCs value of 1.10 ± 0.66 ppbv.

Flight 14, which sampled both the Yellow Sea and the SMA during a high $PM_{2.5}$ transport (Kim et al., 2026), showed an elevated Σ_7VOCs value of 3.19 ± 1.86 ppbv, lower only than the three SMA-focused flights. However, its toluene-to-benzene ratio was substantially lower than those observed during the SMA-focused flights (Table S2), suggesting a larger influence of regionally transported or aged air masses relative to fresh aromatic emissions. Among the remaining flights, benzene was relatively enhanced during Flights 2, 12, and 13, with flight-mean values of 0.29, 0.26, and 0.24 ppbv, respectively, compared with the campaign mean of 0.20 ± 0.08 ppbv. Flight-specific variations in the seven target VOC species or groups are shown in Fig. S1.

During the campaign, the NASA DC-8 also conducted observations over inland Korea and the Yellow Sea on 17 February, 26 February, 8 March, and 10 March 2024. The DC-8 observations from these dates are discussed further in Sect. 4 together with the 1900D results. The corresponding flight tracks, altitude sampling distributions, and vertical profiles of selected VOCs are provided in Figs. S2 and S3. The flight-mean relationships among VOCs also indicate distinct behavior among species. Toluene, C_8 aromatics, and the MEK-equivalent signal varied coherently across flights, with toluene most strongly correlated with C_8 aromatics (r^2 = 0.982). In contrast, the relationship between toluene and benzene was weaker (r^2 = 0.504), and the toluene-to-benzene ratio increased with increasing Σ_7VOCs, indicating that benzene and toluene were affected differently by source composition and atmospheric processing. Benzene showed weaker variability than the more reactive aromatic VOCs and was moderately associated with acetone, consistent with a larger regional background component.

Overall, the campaign observations show that VOC variability was controlled not only by local source strength within the SMA but also by species-dependent atmospheric lifetime and regional transport over the Yellow Sea. The following sections examine these controls using vertical distributions, regional contrasts, inter-species relationships, and transport-related diagnostics.

https://doi.org/10.5194/egusphere-2026-6595
Preprint. Discussion started: 10 November 2026
© Author(s) 2026. CC BY 4.0 License.

Table 2: Summary of flight-specific VOC mixing ratios (mean ± standard deviation, in ppbv) measured during 17 Beechcraft 1900D research flights (F1–F17) during ASIA-AQ. The flights covered various regions, including the Seoul Metropolitan Area (SMA), the Yellow Sea (YS), and Gyeonggi Province (GG). The prevailing winds for each flight are also included.

Flight				VOC mixing ratio mean and standard deviation (ppbv)			
Number	Date	Region	Prevailing winds	C_8 aromatics	MEK-equiv.	Toluene	Benzene
F1	6 Feb	SMA	NW	0.04 ± 0.05	0.14 ± 0.06	0.11 ± 0.12	0.09 ± 0.06
F2	7 Feb	SMA & YS	N	0.08 ± 0.12	0.29 ± 0.33	0.25 ± 0.42	0.29 ± 0.10
F3	8 Feb	SMA	W	0.43 ± 0.21	1.29 ± 1.04	1.92 ± 1.08	0.42 ± 0.11
F4	14 Feb	SMA	SW	0.25 ± 0.18	0.94 ± 0.79	0.97 ± 0.80	0.18 ± 0.11
F5	17 Feb	SMA & YS	S	0.08 ± 0.10	0.36 ± 0.44	0.27 ± 0.46	0.14 ± 0.09
F6	17 Feb	SMA	SW	0.33 ± 0.15	1.41 ± 0.65	1.20 ± 0.59	0.26 ± 0.09
F7	23 Feb	SMA & YS	NE	0.13 ± 0.14	0.51 ± 0.54	0.47 ± 0.59	0.16 ± 0.08
F8	26 Feb	SMA & YS	N	0.08 ± 0.10	0.35 ± 0.26	0.31 ± 0.45	0.21 ± 0.09
F9	28 Feb	SMA & YS	N	0.09 ± 0.18	0.43 ± 0.89	0.37 ± 0.91	0.13 ± 0.10
F10	2 Mar	SMA & YS	SW	0.08 ± 0.07	0.23 ± 0.16	0.16 ± 0.22	0.15 ± 0.08
F11	2 Mar	GG & YS	W	0.05 ± 0.08	0.23 ± 0.06	0.11 ± 0.04	0.18 ± 0.07
F12	3 Mar	SMA & YS	W	0.08 ± 0.05	0.32 ± 0.08	0.20 ± 0.10	0.26 ± 0.13
F13	3 Mar	SMA & YS	W	0.07 ± 0.06	0.36 ± 0.13	0.18 ± 0.11	0.24 ± 0.09
F14	4 Mar	SMA & YS	SE	0.13 ± 0.23	0.79 ± 1.26	0.54 ± 1.20	0.22 ± 0.13
F15	7 Mar	GG & YS	NW	0.05 ± 0.05	0.32 ± 0.25	0.15 ± 0.21	0.17 ± 0.07
F16	8 Mar	SMA & YS	NW	0.05 ± 0.04	0.24 ± 0.12	0.13 ± 0.19	0.13 ± 0.04
F17	10 Mar	YS	SW	0.03 ± 0.01	0.22 ± 0.09	0.07 ± 0.04	0.11 ± 0.05
Average				0.12 ± 0.11	0.50 ± 0.38	0.44 ± 0.49	0.20 ± 0.08

https://doi.org/10.5194/egusphere-2026-6595
Preprint. Discussion started: 10 November 2026
© Author(s) 2026. CC BY 4.0 License.

275 **Table 2. Continued.**

Flight				VOC mixing ratio mean and standard deviation (ppbv)			
Number	**Date**	**Region**	**Prevailing winds**	**Acetonitrile**	**Trimethyl-benzenes**	**Acetone**	**Σ₇VOCs**
F1	6 Feb	SMA	NW	0.08 ± 0.15	0.19 ± 0.21	0.46 ± 0.58	1.10 ± 0.66
F2	7 Feb	SMA & YS	N	0.10 ± 0.04	0.18 ± 0.14	0.69 ± 0.35	1.88 ± 0.67
F3	8 Feb	SMA	W	0.13 ± 0.08	0.44 ± 0.18	1.49 ± 0.68	6.12 ± 1.67
F4	14 Feb	SMA	SW	0.10 ± 0.13	0.28 ± 0.17	1.05 ± 0.79	3.77 ± 1.40
F5	17 Feb	SMA & YS	S	0.07 ± 0.02	0.16 ± 0.10	0.62 ± 0.32	1.69 ± 0.73
F6	17 Feb	SMA	SW	0.10 ± 0.02	0.32 ± 0.11	1.49 ± 0.48	5.10 ± 1.02
F7	23 Feb	SMA & YS	NE	0.07 ± 0.02	0.20 ± 0.12	0.64 ± 0.30	2.18 ± 0.87
F8	26 Feb	SMA & YS	N	0.08 ± 0.03	0.16 ± 0.07	0.76 ± 0.31	1.95 ± 0.62
F9	28 Feb	SMA & YS	N	0.07 ± 0.04	0.18 ± 0.17	0.59 ± 0.42	1.85 ± 1.36
F10	2 Mar	SMA & YS	SW	0.08 ± 0.02	0.14 ± 0.07	0.60 ± 0.16	1.43 ± 0.34
F11	2 Mar	GG & YS	W	0.08 ± 0.02	0.11 ± 0.03	0.71 ± 0.18	1.47 ± 0.22
F12	3 Mar	SMA & YS	W	0.10 ± 0.03	0.16 ± 0.06	0.92 ± 0.35	2.04 ± 0.40
F13	3 Mar	SMA & YS	W	0.09 ± 0.03	0.14 ± 0.05	1.03 ± 0.30	2.11 ± 0.36
F14	4 Mar	SMA & YS	SE	0.10 ± 0.03	0.19 ± 0.17	1.23 ± 0.59	3.19 ± 1.86
F15	7 Mar	GG & YS	NW	0.09 ± 0.02	0.13 ± 0.05	0.91 ± 0.32	1.81 ± 0.47
F16	8 Mar	SMA & YS	NW	0.08 ± 0.02	0.13 ± 0.09	0.73 ± 0.24	1.48 ± 0.34
F17	10 Mar	YS	SW	0.08 ± 0.02	0.10 ± 0.03	0.74 ± 0.25	1.35 ± 0.27
Average				0.09 ± 0.02	0.19 ± 0.09	0.86 ± 0.31	2.38 ± 1.39

https://doi.org/10.5194/egusphere-2026-6595
Preprint. Discussion started: 10 November 2026
© Author(s) 2026. CC BY 4.0 License.

3.2 Characteristic distributions of VOCs

3.2.1 Vertical distribution

To examine how VOC distributions differed between source-influenced and marine air masses, vertical profiles were constructed for the entire 1900D campaign after classifying observations into land and sea categories using the Korean coastline boundary (Fig. 2). The analysis focused on six representative target VOCs: toluene, C_8 aromatics, MEK-equivalent signal, benzene, acetone, and acetonitrile.

Toluene, C_8 aromatics, and the MEK-equivalent signal showed pronounced enhancements within the lower troposphere over land. Across the analyzed altitude range (200–3000 m), their mean mixing ratios over land were 0.90 ± 1.00 ppbv for toluene, 0.23 ± 0.21 ppbv for C_8 aromatics, and 0.82 ± 0.90 ppbv for MEK-equivalent signal. The corresponding mean mixing ratios over sea were substantially lower, at 0.18 ± 0.38 ppbv, 0.06 ± 0.09 ppbv, and 0.31 ± 0.38 ppbv, respectively. These land–sea contrasts indicate that the more reactive aromatic VOCs and MEK-equivalent signal were strongly influenced by low-altitude source regions over the SMA and adjacent western coastal corridor.

Although their campaign-mean concentrations were higher over land, high mixing ratios of toluene, MEK-equivalent signal, and C_8 aromatics were also observed in low-altitude marine or coastal air masses near 300 m, with peak values of 8.7, 9.2, and 2.0 ppbv, respectively (Fig. 2). These maxima were not representative of the marine background but instead reflected episodic plume encounters near the western coastal industrial corridor and adjacent marine region. The large variability within individual altitude bins, reflected by the 1σ error bars in Fig. 2, further indicates that these short-lived or source-sensitive VOCs were affected by intermittent plume sampling rather than by a uniformly enhanced background over the sea.

Benzene and acetone showed weaker land–sea contrasts than toluene, C_8 aromatics, and MEK-equivalent signal. Mean benzene mixing ratios were 0.24 ± 0.15 ppbv over land and 0.18 ± 0.09 ppbv over the sea, while acetone mixing ratios were 1.07 ± 0.68 ppbv and 0.77 ± 0.31 ppbv, respectively. Benzene remained elevated up to approximately 900–1000 m over land and generally exhibited a weaker vertical gradient than the more reactive aromatic VOCs.

Across the operational PBL threshold of 1100 m, benzene decreased from 0.25 ± 0.15 within the PBL to 0.08 ± 0.06 ppbv above the PBL over land, corresponding to a reduction of about 70 %. Over the Yellow Sea, however, the decrease was much weaker, from 0.19 ± 0.09 to 0.15 ± 0.07 ppbv, corresponding to a reduction of about 21 %. Elevated benzene was also observed near 2000 m over the Yellow Sea, and back trajectory analysis of these observations showed air mass pathways extending toward continental regions to the west and northwest, consistent with transported continental influence at these altitudes (Fig. S4).

Acetone, the most abundant target VOC during the campaign, also decreased with altitude over land, from 1.10 ± 0.68 ppbv within the PBL to 0.41 ± 0.22 ppbv above the PBL. Over the sea, acetone showed weaker vertical variability and remained near 0.82 ± 0.25 ppbv above the PBL. This behavior is consistent with the relatively long atmospheric lifetime of acetone and the contribution of regional and secondary sources (Singh et al., 2004).

Acetonitrile showed the weakest vertical and land–sea variability among the measured VOCs. Mean concentrations were similar over land and sea, at 0.095 ± 0.077 and 0.084 ± 0.024 ppbv, respectively. Occasional enhancements below approximately 1000 m over land may reflect localized plume influences, but the overall

https://doi.org/10.5194/egusphere-2026-6595
Preprint. Discussion started: 10 November 2026
© Author(s) 2026. CC BY 4.0 License.

315 weak vertical and regional gradients indicate that acetonitrile was dominated by a regional background component during the campaign.

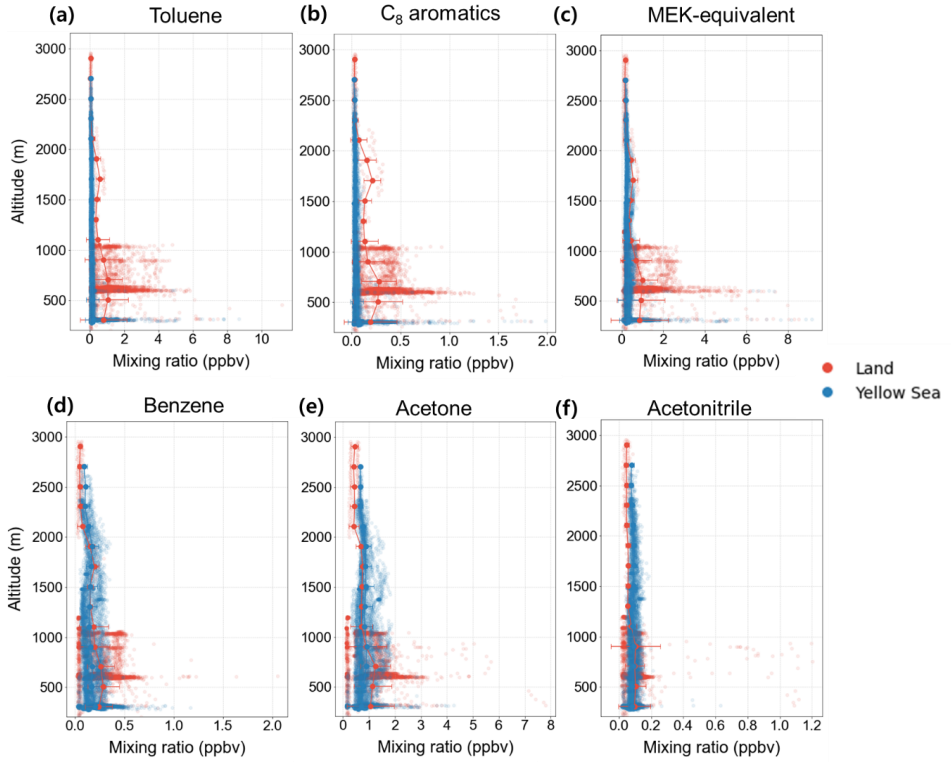


Figure 2: Vertical profiles of major VOCs (toluene, C_8 aromatics, MEK-equivalent signal, benzene, acetone and acetonitrile) measured by the 1900D aircraft over the entire campaign period. VOC mixing ratios (ppbv) are separated 320 **into land (red) and Yellow Sea (blue) observations, with the classification based on the Korean coastline boundary. Bold lines and markers indicate mean values calculated within 200-m altitude intervals; error bars represent one standard deviation (1 σ) of the observations within each interval.**

Together, the vertical profiles show a clear contrast between short-lived, source-sensitive VOCs and longer-lived or more regionally mixed compounds. Toluene, C_8 aromatics, and MEK-equivalent signal were strongly enhanced 325 in low-altitude source-influenced air masses, whereas benzene, acetone, and acetonitrile showed weaker land–sea contrasts and more persistent vertical distributions, particularly over the Yellow Sea.

3.2.2 Geographical distributions

The vertical profiles demonstrated that several VOCs were strongly enhanced in low-altitude source-influenced 330 air masses. To further examine regional differences in VOC composition, we compared observations within the PBL between the Seoul region and the Yellow Sea. The Seoul region was defined as 37.4–37.7° N and 126.7–127.2° E, while the Yellow Sea region was defined as 36.0–38.0° N and 124.0–125.5° E, excluding the western coastal industrial corridor.

https://doi.org/10.5194/egusphere-2026-6595
Preprint. Discussion started: 10 November 2026
© Author(s) 2026. CC BY 4.0 License.

Mean Σ_7VOCs mixing ratios were 3.66 ± 2.44 ppbv over Seoul and 1.55 ± 0.50 ppbv over the Yellow Sea, indicating that Seoul concentrations were approximately 2.4 times higher. Acetone was the most abundant target VOC in both regions, with mean concentrations of 1.07 ± 0.58 ppbv over Seoul and 0.77 ± 0.30 ppbv over the Yellow Sea. In Seoul, acetone was followed by toluene (0.96 ± 0.95 ppbv) and MEK-equivalent signal (0.75 ± 0.61 ppbv), whereas over the Yellow Sea it was followed by MEK-equivalent signal (0.26 ± 0.10 ppbv) and benzene (0.18 ± 0.09 ppbv).

The VOC composition differed substantially between the two regions. Over Seoul, toluene was comparable to acetone and represented a major component of Σ_7VOCs. Over the Yellow Sea, acetone accounted for nearly half of Σ_7VOCs, and benzene contributed a larger fraction than over Seoul. In contrast, toluene and C_8 aromatics were much lower over the Yellow Sea, consistent with dilution, chemical aging, and weaker influence from fresh aromatic emissions (Parrish et al., 2007; Warneke et al., 2013). Among the measured VOCs, acetonitrile showed the smallest regional difference, with mean concentrations of 0.10 ± 0.07 ppbv over Seoul and 0.09 ± 0.02 ppbv over the Yellow Sea. This weak regional contrast suggests that acetonitrile largely represented a regional background component during the campaign, with only limited influence from localized plume events.

Ground-based measurements at the Korea University campus in Seoul (37.585° N, 127.026° E) provide additional context for the airborne observations (Table 3). Because the ground site represents a fixed urban surface location, whereas the aircraft sampled a broader metropolitan domain including the southwestern industrial corridor, direct comparison should be interpreted qualitatively. Ground-based mixing ratios were generally higher than those observed in the Seoul airborne measurements for most species, consistent with stronger near-surface source influence at the fixed urban site. MEK was lower at the ground site, with a mean mixing ratio of 0.34 ± 0.36 ppbv compared with 0.75 ± 0.61 ppbv for the airborne MEK-equivalent signal. This difference suggests that the airborne observations over Seoul captured MEK-equivalent enhancements associated with broader metropolitan and coastal industrial plume influences that were not fully represented at the fixed Korea University site.

Overall, the regional comparison reinforces the vertical profile results. Toluene, C_8 aromatics, and MEK-equivalent signal were strongly enhanced over Seoul and source-influenced low-altitude air masses, whereas benzene, acetone, and acetonitrile showed weaker Seoul–Yellow Sea contrasts. These differences provide the observational basis for examining VOC source signatures and lifetime-dependent variability in the following sections.

https://doi.org/10.5194/egusphere-2026-6595
Preprint. Discussion started: 10 November 2026
© Author(s) 2026. CC BY 4.0 License.

Table 3: VOC mixing ratios observed over the Yellow Sea (36–38° N, 124–125.5° E), Seoul (37.4–37.7° N, 126.7–127.2° E), and at the ground-based Korea University site (37.585° N, 127.026° E). Values are given as mean ± standard deviation, median, and maximum for the airborne observations, and as mean ± standard deviation for the ground-based measurements. Dash indicates a value not reported.

	Yellow Sea (ppbv)			Seoul (ppbv)			Ground (ppbv)
Species	Mean	Median	Max	Mean	Median	Max	Mean
C_8 aromatics	0.04 ± 0.02	0.04	0.53	0.24 ± 0.20	0.21	1.11	0.81 ± 0.73
MEK-equivalent	0.26 ± 0.10	0.23	0.85	0.75 ± 0.61	0.54	2.82	0.34 ± 0.36
Toluene	0.11 ± 0.07	0.10	1.10	0.96 ± 0.95	0.69	4.79	1.79 ± 1.77
Benzene	0.18 ± 0.09	0.15	0.86	0.28 ± 0.15	0.24	1.18	0.51 ± 0.21
Acetonitrile	0.09 ± 0.02	0.08	0.46	0.10 ± 0.07	0.09	1.20	0.33 ± 0.15
Trimethylbenzenes	0.12 ± 0.04	0.12	0.74	0.28 ± 0.17	0.25	1.62	0.11 ± 0.11
Acetone	0.77 ± 0.30	0.71	2.84	1.07 ± 0.58	1.09	5.70	2.32 ± 1.67
Σ_7VOCs	1.55 ± 0.50	—	—	3.66 ± 2.44	—	—	—

3.3 Source signatures of VOCs

3.3.1 Inter-species relationships

The vertical and geographical distributions presented in Sect. 3.2 show that toluene, C_8 aromatics, and MEK-equivalent signal were strongly enhanced over the Seoul Metropolitan Area (SMA) and in low-altitude coastal or inland plumes, whereas benzene exhibited a weaker land–sea contrast. To further examine the roles of source composition and atmospheric processing, inter-species relationships were analyzed for observations within the operational PBL (<1100 m). Observations were classified into four regions: Seoul, southern inland, coastal, and Yellow Sea. The coastal region included the western industrial corridor extending from the Ansan–Sihwa industrial complex toward the Daesan petrochemical complex, where industrial VOC emissions have been reported previously (Fried et al., 2020; Kim et al., 2020; Sarkar et al., 2021; Shin et al., 2024).

Benzene and toluene were used as reference species because they represent different atmospheric lifetimes and source characteristics. Benzene has a longer atmospheric lifetime than the more reactive aromatics and therefore provides a useful reference for more regionally persistent combustion-related or aged air masses (Atkinson, 2000; Parrish et al., 2007). Toluene is more reactive and more sensitive to fresh aromatic emissions, including traffic and solvent-related sources (Warneke et al., 2013; Yuan et al., 2010). MEK-equivalent signal represents a mixed oxygenated VOC signal that may include contributions from both direct emissions and secondary formation (Singh et al., 2004).

The inter-species relationships differed substantially by region and reference species (Fig. 3). When benzene was used as the reference species, C_8 aromatics over Seoul formed a relatively compact relationship (slope = 1.11 ± 0.02, r^2 = 0.65; Fig. 3a), whereas toluene and MEK-equivalent signal showed broader and more structured distributions. The MEK-equivalent-to-benzene slope also showed a strong regional contrast, with a slope of 2.41 over Seoul compared with 0.65 over the Yellow Sea. These contrasts indicate that toluene and MEK-equivalent signal were strongly enhanced relative to benzene in source-influenced air masses over the SMA.

When toluene was used as the reference species, C_8 aromatics showed clearer separation within the Seoul observations. This behavior is consistent with varying aromatic source mixtures within the metropolitan region. In particular, enhanced toluene and C_8 aromatics together are consistent with non-combustion aromatic emissions,

https://doi.org/10.5194/egusphere-2026-6595
Preprint. Discussion started: 10 November 2026
© Author(s) 2026. CC BY 4.0 License.

including potential solvent-related contributions, in addition to traffic-related sources (Simpson et al., 2020). In the MEK-equivalent relationships (Fig. 3d, e), some Seoul observations showed continuity with coastal and southern inland observations, suggesting that part of the Seoul-domain MEK-equivalent enhancement was associated with air masses influenced by the broader western coastal industrial corridor.

In contrast, Yellow Sea observations were concentrated within lower concentration ranges for most inter-species relationships. This pattern indicates weaker influence from fresh local aromatic emissions and a larger contribution from aged or regionally mixed air masses. Acetonitrile exhibited broadly dispersed distributions without clear regional separation. Although several high-concentration points extended from Seoul and coastal regions, the overall weak regional structure suggests that acetonitrile was dominated by a regional background component during the campaign, with occasional localized plume influence.

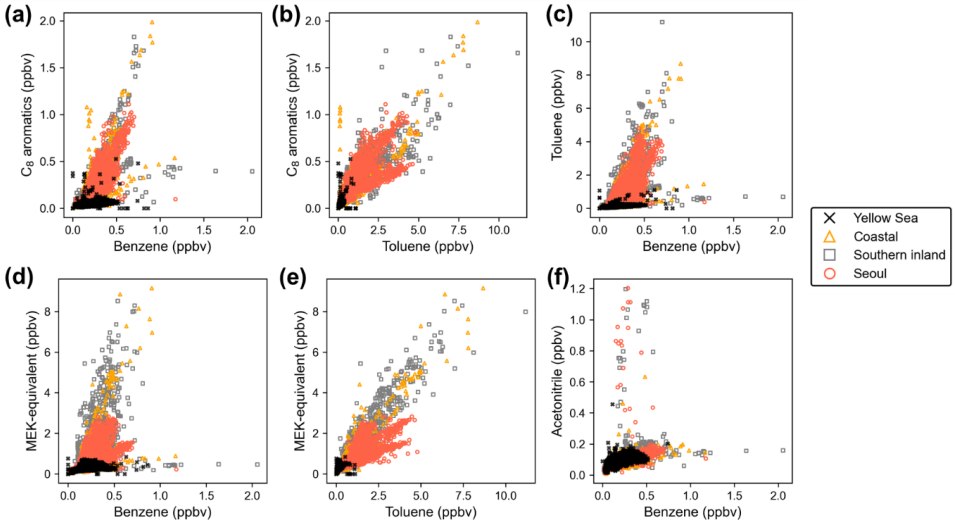


Figure 3: Relationships among major VOC species using benzene and toluene as reference variables for 1900D observations during ASIA-AQ. Observations within the PBL (<1100 m) are classified into the Yellow Sea, coastal, southern inland, and Seoul Metropolitan Area (SMA) regions. Panels show (a) C_8 aromatics–benzene, (b) C_8 aromatics–toluene, (c) toluene–benzene, (d) MEK-equivalent–benzene, (e) MEK-equivalent–toluene, and (f) acetonitrile–benzene relationships.

Hourly distributions of C_8 aromatics, toluene, MEK-equivalent signal, and benzene within the SMA PBL provided additional context for the observed source-sensitive variability (Fig. 4). These distributions should be interpreted as hour-of-day distributions from sampled flight periods rather than as a complete diurnal cycle. C_8 aromatics increased around midday and then decreased during the afternoon, whereas toluene showed the largest variability and episodic enhancements after noon. MEK-equivalent signal increased during a similar period but remained elevated for a broader portion of the afternoon. Benzene showed the weakest hourly variability, consistent with its longer lifetime and larger regional background contribution.

Together, the inter-species and hourly distributions indicate that VOC variability within the SMA PBL was not controlled solely by boundary-layer dilution. Instead, the observed relationships reflect a combination of source composition, atmospheric lifetime, and intermittent sampling of source-influenced plumes. The stronger

https://doi.org/10.5194/egusphere-2026-6595
Preprint. Discussion started: 10 November 2026
© Author(s) 2026. CC BY 4.0 License.

enhancement of toluene, C_8 aromatics, and MEK-equivalent signal relative to benzene points to fresh or recently emitted VOC mixtures within the SMA and adjacent western coastal corridor.

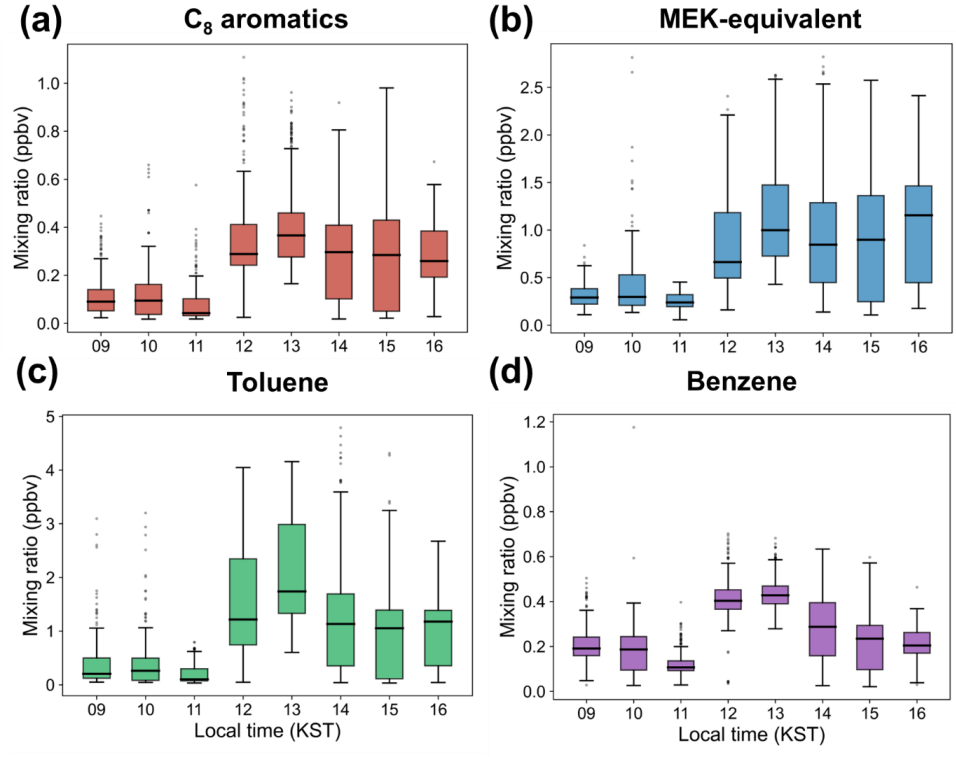


Figure 4: Hourly distribution of VOC mixing ratios within the planetary boundary layer (PBL; <1100 m) over the Seoul Metropolitan Area (SMA) during the ASIA-AQ winter campaign. Boxplots represent hourly distributions of (a) C_8 aromatics, (b) MEK-equivalent, (c) toluene, and (d) benzene using 1 h bins in local time (KST). Boxes indicate the interquartile range (25th–75th percentiles), horizontal lines denote medians, and points indicate outliers.

3.3.2 Variability in relation to photochemical lifetime

To evaluate whether the regional VOC contrasts were related to atmospheric reactivity, we compared the Seoul-to-Yellow Sea ratio of VOC-to-benzene regression slopes, defined as $(\Delta VOC_i/\Delta Benzene)_{Seoul}/(\Delta VOC_i/\Delta Benzene)_{YS}$, with $1/\tau$ (Fig. 5). The lifetimes were calculated using OH reaction rate constants and a fixed 12-h daytime average OH concentration of 2.0×10^6 molecules cm^{-3}, representative of wintertime urban and suburban photochemical conditions (Kanaya et al., 2007; Ren et al., 2006; Stone et al., 2012). The $1/\tau$ value was used as a relative reactivity indicator, with larger values corresponding to shorter-lived and more reactive VOCs. The OH reaction rate constants and representative lifetimes used in this analysis are summarized in Table S4.

Overall, the Seoul-to-Yellow Sea slope ratio increased with $1/\tau$, indicating that more reactive VOCs generally showed stronger regional contrasts. The empirical relationship was expressed as $R_i = 2.06 \log_{10}[(1/\tau_i)/(1\ d^{-1})] +$

https://doi.org/10.5194/egusphere-2026-6595
Preprint. Discussion started: 10 November 2026
© Author(s) 2026. CC BY 4.0 License.

5.90, where R_i is the Seoul-to-Yellow Sea slope ratio. The fit explained part of the observed variability ($r^2 = 0.42$), indicating that atmospheric lifetime contributed to the regional differences among VOCs. However, this relationship should be interpreted as an empirical trend rather than as a direct representation of chemical loss, because the observed ratios also reflect differences in emission source composition, dilution, and transport pathways.

Longer-lived compounds generally showed smaller regional contrasts. Acetone and acetonitrile had low slope ratios of 1.70 ± 0.05 and 1.10 ± 0.06, respectively, consistent with their relatively weak Seoul–Yellow Sea gradients. The MEK-equivalent signal showed an intermediate ratio of 3.7 ± 0.1, consistent with its mixed source characteristics. In contrast, toluene and C_8 aromatics showed positive deviations from the fitted reactivity trend. Their observed slope ratios were 11.3 ± 0.3 and 9.3 ± 0.2, respectively, compared with their fitted values of approximately 5.2 and 6.1 at their corresponding $1/\tau$ values. Toluene showed the largest Seoul-to-Yellow Sea slope ratio despite having a longer lifetime than C_8 aromatics, indicating that its distribution was strongly influenced by source composition in addition to atmospheric reactivity. The elevated ratio of C_8 aromatics similarly supports the influence of fresh or recently emitted aromatic VOCs within the SMA.

The trimethylbenzenes, represented by a lifetime of 0.3 days in the fit, showed a lower ratio of 5.6 ± 0.2 and fell below the fitted trend. This deviation further indicates that differences among reactive aromatic VOCs cannot be explained solely by OH reactivity. The lower-than-expected trimethylbenzene ratio may reflect larger measurement uncertainty, because trimethylbenzenes were not directly calibrated, as well as differences in source composition and rapid dilution of localized plumes.

This relative enrichment of toluene in Seoul is also reflected in the toluene-to-benzene (T/B) ratio. Within the SMA PBL, the mean T/B ratio was 5.14 ± 2.52, about 30 % lower than the value of 7.6 ± 4.9 reported below 500 m during the 2016 KORUS-AQ campaign (Simpson et al., 2020), but the mean ± SD intervals overlapped. Although KORUS-AQ was conducted in May–June and the present observations were made in winter, the overlapping ranges indicate that toluene remained strongly enhanced relative to benzene in Seoul during ASIA-AQ. In contrast, ship-based observations over the Yellow Sea reported T/B ratios close to unity (Wang et al., 2023), consistent with a more aged marine background. These results show that the Seoul-to-Yellow Sea contrast reflects both reactivity-dependent processing and source-specific emissions. Atmospheric lifetime helps explain the weaker gradients of longer-lived compounds such as acetone and acetonitrile, whereas the positive deviations of toluene and C_8 aromatics indicate additional influence from urban aromatic source signatures. Therefore, the regional VOC distributions observed during ASIA-AQ were shaped jointly by chemical lifetime, source composition, and transport history.

https://doi.org/10.5194/egusphere-2026-6595
Preprint. Discussion started: 10 November 2026
© Author(s) 2026. CC BY 4.0 License.

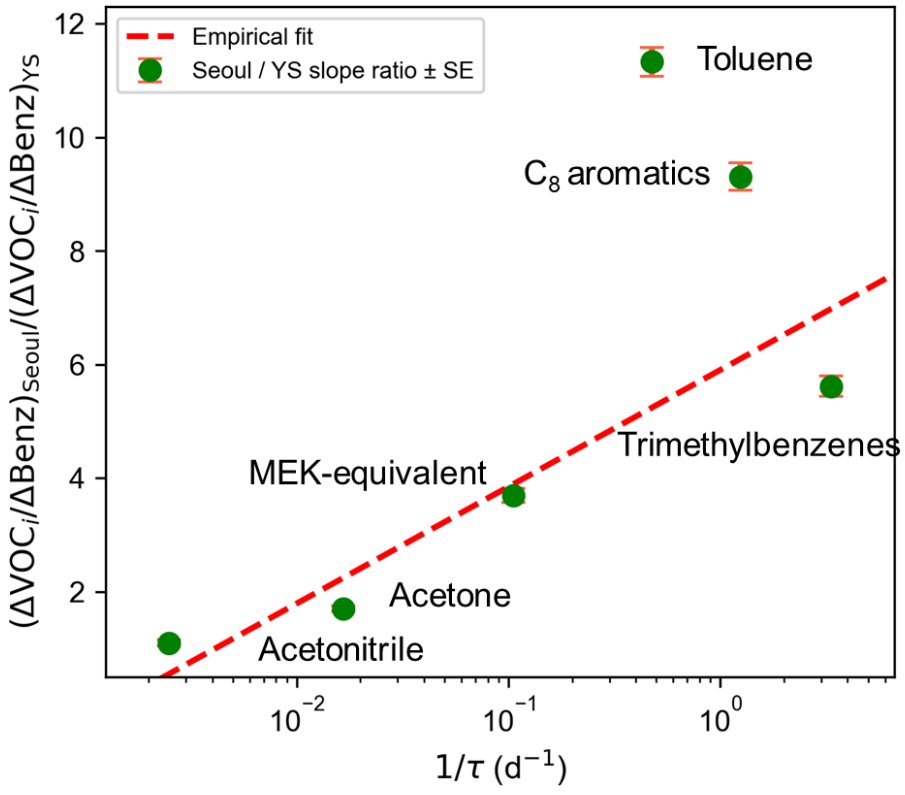


Figure 5: Regression slope ratio between Seoul and the Yellow Sea as a function of 1/τ. The ratio is defined as $(\Delta VOC_i/\Delta Benzene)_{Seoul}/(\Delta VOC_i/\Delta Benzene)_{YS}$. Green markers indicate the slope ratios with propagated standard errors, and the red dashed line shows the empirical fit $R_i = 2.06 \log_{10}[(1/\tau_i)/(1\ d^{-1})] + 5.90$ ($r^2 = 0.42$). OH-reaction rate constants and representative lifetimes are provided in Table S4.

3.4 Comparison with CAPSS emission inventory

To examine whether the VOC spatial patterns observed by the 1900D were broadly consistent with available emission information, we compared selected airborne observations with the 2021 Clean Air Policy Support System (CAPSS) emission inventory over the SMA (Fig. 6). This comparison is intended as a qualitative source-context analysis rather than a direct evaluation of the inventory. CAPSS represents annual, surface-level bottom-up emissions, whereas the 1900D observations represent selected wintertime flight periods at varying altitudes. Therefore, differences between the two datasets can reflect not only emission uncertainties but also differences in season, sampling altitude, meteorology, chemical processing, and temporal representativeness.

The comparison focused on toluene and benzene because these two species showed contrasting behavior in the 1900D observations. Toluene was strongly enhanced over Seoul and showed large positive deviation from the lifetime-based regional trend, indicating strong sensitivity to source composition. Benzene, in contrast, exhibited

https://doi.org/10.5194/egusphere-2026-6595
Preprint. Discussion started: 10 November 2026
© Author(s) 2026. CC BY 4.0 License.

weaker spatial variability and a larger regional background component. For toluene, the CAPSS field shown in Fig. 6 represents the SAPRC07 ARO1 lumped aromatic category, which includes lower-reactivity aromatics, primarily toluene and other monosubstituted benzenes. The comparison should therefore be interpreted as a toluene-related aromatic source context, not as a one-to-one comparison with measured toluene.

CAPSS ARO1 emissions showed several prominent source regions within and around Seoul, including central Seoul, the northwestern suburban area near Goyang and Paju (Kim, 2024; Lee et al., 2022), and southeastern Seoul. Elevated airborne toluene concentrations were frequently observed over central and southeastern Seoul, broadly consistent with these inventory hotspots. The southeastern enhancement is also consistent with reported local source information, including automobile painting facilities and other urban-industrial activities in this part of the metropolitan area (Chun et al., 2021; Lee et al., 2024). In contrast, the 1900D flight tracks passed south of the northwestern Goyang-Paju hotspot and were generally at higher altitude over western Seoul than over southeastern Seoul. These sampling differences likely reduced the sensitivity of the aircraft observations to near-surface emissions in the northwestern hotspot.

Benzene showed a more spatially uniform distribution across the SMA than toluene. This pattern is consistent with the longer atmospheric lifetime of benzene and its larger regional background contribution inferred from the vertical and regional distributions. The weaker spatial correspondence between airborne benzene and localized CAPSS emission features therefore does not necessarily imply disagreement with the inventory; rather, it reflects the stronger influence of atmospheric persistence, dilution, and regional mixing on the observed benzene field. Temporal differences between the inventory year and the ASIA-AQ observations provide an additional limitation. CAPSS data used here correspond to 2021, whereas the airborne observations were conducted in February–March 2024. Ground-based PAMS statistics indicate that VOC levels changed between 2021 and later years. For example, at Jung-gu in central Seoul, mean toluene increased from 4.2 ppbv in 2021 to 5.2 ppbv in 2023, whereas mean toluene at Bucheon decreased from 2.7 ppbv to 1.7 ppbv over the same period (NIER, 2024). These changes indicate that discrepancies between CAPSS and airborne observations may partly reflect changes in VOC emissions or concentrations after the inventory year, in addition to spatial allocation and altitude-sampling differences.

Overall, the CAPSS comparison supports the interpretation that toluene was strongly influenced by localized urban and industrial aromatic sources, whereas benzene reflected a more regionally mixed component. The airborne observations captured localized and temporally variable VOC enhancements that are difficult to represent fully in an annual surface emission inventory. Thus, results indicate that the 1900D data provide complementary observational constraints on the spatial heterogeneity of VOC source influences over the SMA, while the CAPSS inventory provides useful source context for interpreting the observed aromatic VOC patterns.

https://doi.org/10.5194/egusphere-2026-6595
Preprint. Discussion started: 10 November 2026
© Author(s) 2026. CC BY 4.0 License.

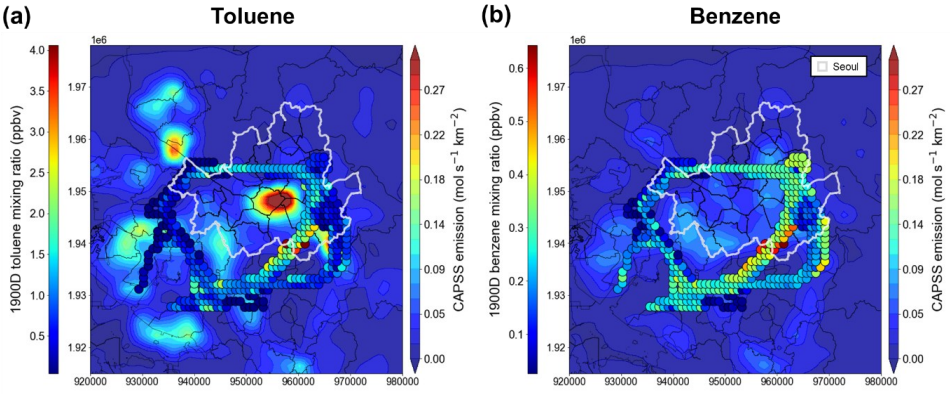


Figure 6: Comparison of airborne observations (points; February–March 2024) and inventory-based (background; 2021) VOC distributions over the Seoul Metropolitan Area for (a) toluene and (b) benzene. Background color maps represent 2021 CAPSS emission inventory data (mol s⁻¹ km⁻²). Panel (a) shows the SAPRC07 ARO1 lumped aromatic category, which includes toluene and other lower-reactivity aromatic compounds, whereas panel (b) shows the benzene emission field. Overlaid scatter points indicate VOC mixing ratios (ppbv) measured from all 1900D flights over the SMA during ASIA-AQ. White lines indicate administrative boundaries of Seoul. Both axes are shown in Universal Transverse Mercator (UTM) coordinates.

3.5 Estimation of eastward VOC transport across the Yellow Sea

The preceding sections showed that benzene and toluene exhibited contrasting spatial behavior. Toluene was strongly enhanced within the SMA and in low-altitude coastal or inland plumes, whereas benzene showed weaker spatial variability, a larger regional background component, and more persistent concentrations over the Yellow Sea. These differences suggest that regional transport may be more important for longer-lived benzene than for more source-sensitive toluene. Back trajectory analysis of the highest benzene concentration observed over the Yellow Sea on 2 March 2024 showed a clear pathway from continental regions to the west, providing additional support for the regional transport interpretation (Fig. S5). To examine this contrast quantitatively, we estimated the order of magnitude of eastward benzene and toluene transport across the Yellow Sea using the 1900D observations.

The flux calculation was performed at the 124° E meridional cross section using PTR-ToF-MS VOC concentrations and AIMMS wind observations. The calculation was restricted to the operational PBL layer from the surface to 1100 m, because this layer is most directly coupled to near-surface air quality over the Korean Peninsula. The integration was also restricted to the Seoul latitude band from 37.43° N to 37.70° N. For each VOC species, the eastward transport flux was estimated by integrating the product of the interpolated mass concentration field and the eastward wind component across the vertical cross section:

$$F_i = \int_{z_1}^{z_2} \int_{y_s}^{y_n} u\,(y,z) C_i\,(y,z)\; dydz \qquad (1)$$

where $C_i(y,z)$ is the interpolated mass concentration of species i, and $u(y,z)$ is the eastward wind component for grid cells with $u(y,z) > 0$. Grid cells with non-positive wind speeds were excluded from the inflow calculation. The resulting values therefore represent gross eastward transport equivalents across the 124° E section rather than net VOC fluxes or closed receptor budgets for Seoul (Fig. 7).

https://doi.org/10.5194/egusphere-2026-6595
Preprint. Discussion started: 10 November 2026
© Author(s) 2026. CC BY 4.0 License.

Within the PBL and over the Seoul latitude band, the integrated eastward transport equivalents at 124° E were 280 Mg per month for benzene and 250 Mg per month for toluene. These values represent the transport potential across the sampled Yellow Sea section during the campaign period. Because the 124° E section is located offshore, the calculated fluxes cannot be interpreted directly as the amount reaching the Seoul Metropolitan Area. We therefore applied an empirical distance-based scaling to estimate the equivalent transport toward the Korean coast. The scaling factor was derived from the observed offshore-to-coastal concentration gradients (Fig. S6) using the log-linear function in Eq. (2).

$$C_i(d) = C_{i,0} \cdot \exp(k_i d) \quad (2)$$

where d is the geodesic distance from the nearest Korean coastline, $C_i(d)$ is the concentration of species i at distance (d), $C_{i,0}$ is the fitted concentration at the coastline, and k_i is the fitted spatial gradient coefficient. A positive k_i indicates higher fitted concentrations farther offshore and therefore a decrease toward the Korean coast. Because this coefficient was derived from the observed spatial variability, it should be interpreted as an apparent gradient that combines chemical loss, dilution, vertical and horizontal mixing, deposition, and transport variability. It is not a species-specific chemical loss rate.

Applying the fitted coastline-to-124° E concentration ratio to the PBL-integrated transport yielded distance-scaled eastward transport equivalents of 88 Mg per month for benzene and 110 Mg per month for toluene. For source-context comparison, these values were compared with Seoul CAPSS emissions (Table 4). The distance-scaled benzene transport equivalent of 88 Mg per month corresponded to approximately 30 % of Seoul CAPSS benzene emissions, whereas the corresponding value for toluene was approximately 6 %. This contrast indicates that Yellow Sea transport can represent a non-negligible contribution to wintertime benzene loading, while toluene remains more strongly controlled by local and domestic emissions.

The absolute values should be interpreted cautiously. The calculation depends on the operational PBL threshold, limited flight sampling, interpolation across the 124° E cross section, and empirical distance-based scaling. Sensitivity tests using PBL thresholds of 900–1300 m shifted the benzene transport equivalent from 21.5 % to 34.4 % of Seoul CAPSS benzene emissions and the toluene equivalent from 4.9 % to 7.6 % of Seoul CAPSS toluene emissions. Although the distance-scaling regressions showed high r^2 values, the observed distance range was limited, and the fitted gradient may include transport and mixing variability in addition to chemical processing. Despite these uncertainties, the species contrast is robust. Benzene and toluene showed comparable gross eastward transport at 124° E, but their distance-scaled equivalents were very different relative to Seoul emissions because of differences in atmospheric lifetime, domestic emission magnitude, and source localization. The flux analysis therefore supports the broader interpretation from the vertical, regional, and inter-species analyses: longer-lived benzene is more sensitive to regional transport across the Yellow Sea, whereas toluene is more strongly influenced by localized urban and industrial sources within Korea.

https://doi.org/10.5194/egusphere-2026-6595
Preprint. Discussion started: 10 November 2026
© Author(s) 2026. CC BY 4.0 License.

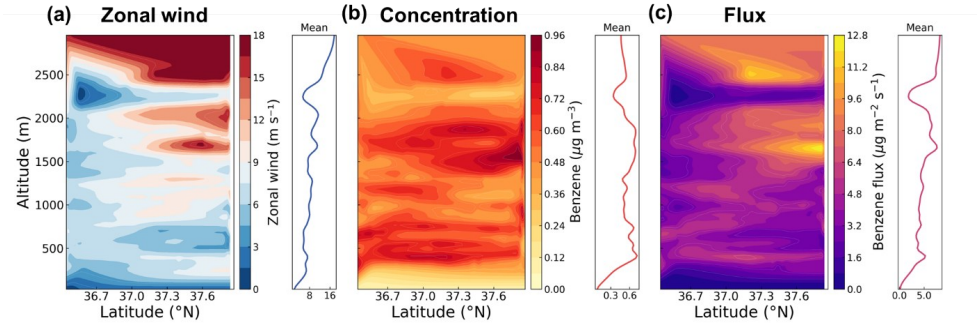


Figure 7: Spatial distribution of (a) zonal wind speed (m s^{-1}), (b) benzene mass concentration (μg m^{-3}), and (c) benzene flux (μg m^{-2} s^{-1}) measured at 124° E. Wind speed was measured by the AIMMS-30 meteorological system onboard the aircraft. The right side of each plot shows mean vertical profiles averaged across latitude: (a) wind speed, (b) benzene concentration, and (c) benzene flux.

Table 4: Comparison of eastward VOC transport equivalents across the Yellow Sea and Seoul CAPSS emissions (unit: Mg per month).

VOC	Eastward transport equivalent at 124° E (0–1100 m)[a]	Distance-scaled eastward transport equivalent (0–1100 m)[b]	Seoul CAPSS emissions[c]
Benzene	280	88	308
Toluene	250	110	1678

[a] The PBL-integrated eastward transport equivalents were calculated at 124° E over 0–1100 m.

[b] The distance-scaled values were estimated using the fitted concentration ratio between the Korean coastline and the 124° E cross section. The distance-scaled values represent equivalent transport toward the Korean coast rather than a direct receptor budget for Seoul.

[c] CAPSS values represent emissions from Seoul.

4 Regional chemical context from NASA DC-8 observations

The 1900D observations provide the primary basis for interpreting wintertime VOC distributions over the Seoul Metropolitan Area (SMA), adjacent western coastal industrial regions, and the Yellow Sea. The preceding sections showed that source-sensitive VOCs, particularly toluene, C_8 aromatics, and MEK-equivalent signal, were strongly enhanced in low-altitude source-influenced air masses, whereas benzene, acetone, and acetonitrile exhibited weaker regional contrasts and more persistent distributions. Here, NASA DC-8 observations collected during the same campaign period are used to place these 1900D-based interpretations within a broader regional and vertical chemical context.

The DC-8 and the 1900D conducted observations over Korea and the Yellow Sea on four common dates during ASIA-AQ, corresponding to five 1900D flights. Because the two aircraft were not co-located in time, altitude, or horizontal position, their observations are interpreted as complementary views of the regional VOC field rather than as paired platform comparisons. The DC-8 sampled broader regional and vertical domains over the Yellow Sea and inland Korea, whereas the 1900D repeatedly sampled lower-altitude air masses within the planetary

https://doi.org/10.5194/egusphere-2026-6595
Preprint. Discussion started: 10 November 2026
© Author(s) 2026. CC BY 4.0 License.

boundary layer over the SMA and adjacent western coastal industrial regions (Figs. 1 and S2). Detailed descriptions of the DC-8 VOC and trace gas measurements used in this analysis are provided in Sect. S3 and Table S3.

The DC-8 CO/CO_2 and O_3/NO_x observations showed distinct chemical phase-space distributions depending on geographic region (Fig. 8a). The O_3/NOx ranges proposed by Morgan et al. (2010) were used as a reference for interpreting chemical gradients associated with differences in source influence and atmospheric processing. Yellow Sea observations occupied a broad portion of the phase space and extended into a distinct higher CO/CO_2 branch, with generally higher O_3/NO_x values than Seoul observations, suggesting differences in source influences and transport histories between the sampled air masses. In contrast, Seoul observations were concentrated primarily under lower O_3/NO_x conditions. These patterns indicate that the Yellow Sea air masses sampled during ASIA-AQ included combustion-influenced continental outflow and regionally processed air masses, whereas Seoul observations more strongly reflected fresher, NO_x-influenced urban conditions.

Within this geographic framework, benzene and toluene showed contrasting distributions in the same chemical phase space (Fig. 8b, c). Benzene enhancements extended toward higher CO/CO_2 values and were observed across a broader range of chemical conditions, including conditions frequently sampled over the Yellow Sea. This behavior is consistent with the longer lifetime of benzene and its association with regionally transported combustion-influenced air. In contrast, the largest toluene mixing ratios were concentrated primarily in lower O_3/NO_x and lower to moderate CO/CO_2 conditions, consistent with fresher source-influenced air masses sampled closer to urban or industrial regions.

This DC-8 chemical context is consistent with the regional contrasts identified from the 1900D observations. The extension of benzene enhancements into the higher CO/CO_2 branch supports the interpretation that benzene was more strongly influenced by regional transport over the Yellow Sea. Conversely, the concentration of high toluene mixing ratios under more source-influenced conditions is consistent with the strong toluene enhancements observed over the SMA and adjacent industrial regions. Taken together, the 1900D and DC-8 observations provide complementary perspectives on wintertime VOC variability over Korea and the Yellow Sea. The 1900D measurements resolved low-altitude source-influenced VOC gradients within the SMA and adjacent coastal industrial corridor, while the DC-8 observations placed these gradients within a broader regional chemical context. The combined evidence supports the central conclusion that wintertime VOC variability over the SMA and Yellow Sea was shaped jointly by chemical lifetime, source specificity, and regional transport. Longer-lived species such as benzene were more sensitive to regional transport and Yellow Sea inflow, whereas shorter-lived aromatic VOCs such as toluene were more strongly controlled by localized urban and industrial emissions.

https://doi.org/10.5194/egusphere-2026-6595
Preprint. Discussion started: 10 November 2026
© Author(s) 2026. CC BY 4.0 License.

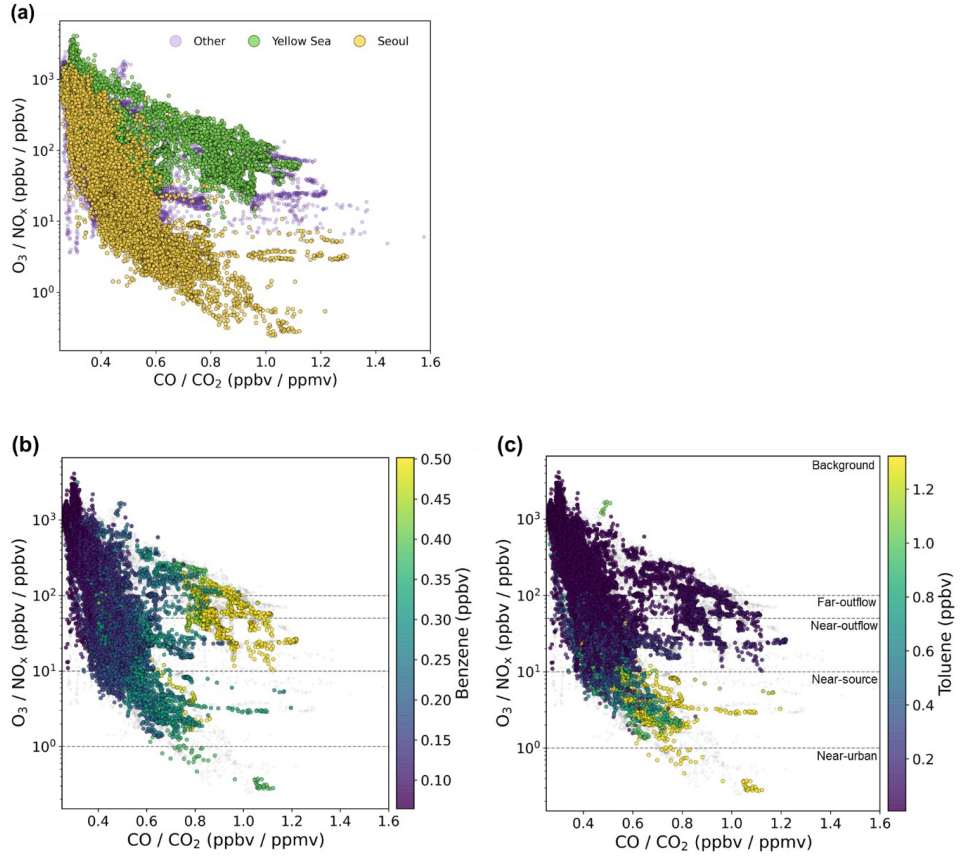


Figure 8: CO/CO_2–O_3/NO_x phase-space distributions from NASA DC-8 observations during the four common flight dates with the 1900D aircraft: 17 February, 26 February, 8 March, and 10 March 2024. Panel (a) shows geographical classification of the DC-8 observations into Yellow Sea, Seoul, and other sampled regions. Panels (b) and (c) show the same phase space colored by Trace Organic Gas Analyzer time-of-flight mass spectrometer (TOGA-TOF) benzene and toluene mixing ratios, respectively. Horizontal dashed lines in panels (b) and (c) indicate O_3/NO_x boundaries of 1, 10, 50, and 100, corresponding to the air mass categories proposed by Morgan et al. (2010): near-urban, near-source, near-outflow, far-outflow, and background. Light-gray points in panels (b) and (c) represent all valid merged DC-8 trace-gas observations, while colored points indicate records with corresponding TOGA-TOF VOC measurements.

5 Conclusions

This study investigated wintertime VOC distributions over the Seoul Metropolitan Area (SMA), adjacent western coastal industrial regions, and the Yellow Sea using high-resolution PTR-ToF-MS observations aboard the 1900D during the ASIA-AQ campaign. The 1900D observations provided repeated low-altitude sampling within the planetary boundary layer, allowing source-influenced VOC gradients over the SMA and nearby industrial regions to be compared with more regionally mixed air masses over the Yellow Sea.

https://doi.org/10.5194/egusphere-2026-6595
Preprint. Discussion started: 10 November 2026
© Author(s) 2026. CC BY 4.0 License.

Mean Σ_7VOCs were approximately 2.4 times higher over Seoul than over the Yellow Sea. Toluene, C_8 aromatics, and MEK-equivalent signal showed strong enhancements within the PBL, particularly in low-altitude source-influenced air masses over urban, coastal and inland regions. By comparison, benzene, acetone, and acetonitrile exhibited weaker contrasts between land and sea, while their vertical distributions were more persistent.

Inter-species relationships further indicated that Seoul VOC enhancements could not be explained by boundary-layer dilution alone. Toluene and C_8 aromatics were strongly enriched relative to benzene over Seoul, whereas Yellow Sea observations were concentrated within lower concentration ranges and showed weaker influence from fresh aromatic emissions. The slope ratios between Seoul and the Yellow Sea generally increased with chemical reactivity, indicating that atmospheric lifetime contributed to the regional VOC contrasts. However, toluene and C_8 aromatics showed positive deviations from this trend, indicating additional influence from urban aromatic source signatures. These results suggest that non-combustion aromatic emissions, including potential solvent-related contributions, remain important for reactive VOC variability in wintertime Seoul. MEK-equivalent enhancements were associated with broader metropolitan, coastal, and southern inland plume influences, although quantitative source apportionment would require additional tracers.

Comparison with the 2021 CAPSS emission inventory provided qualitative source context for the observed aromatic VOC patterns. CAPSS ARO1 emissions showed prominent source regions in central, northwestern, and southeastern parts of the SMA, and elevated airborne toluene concentrations were frequently observed over central and southeastern Seoul. Because CAPSS represents annual surface emissions whereas the aircraft observations represent selected wintertime flight periods at varying altitudes, this comparison should not be interpreted as a direct inventory evaluation. Rather, it indicates that the 1900D observations captured localized and temporally variable aromatic VOC enhancements that are difficult to represent fully in an annual emission inventory.

An order-of-magnitude flux analysis was used to examine the species-dependent role of Yellow Sea transport. Gross eastward transport equivalents calculated at the 124° E cross section were comparable for benzene and toluene, but their distance-scaled transport equivalents differed substantially relative to Seoul CAPSS emissions. The benzene transport equivalent was approximately 30 % of Seoul CAPSS benzene emissions, whereas the corresponding toluene value was approximately 6 % of Seoul CAPSS toluene emissions. These values should be interpreted as order-of-magnitude transport equivalents rather than closed receptor budgets for Seoul, because they depend on the operational PBL threshold, limited flight sampling, interpolation, and empirical distance-based scaling. Nevertheless, the contrast between benzene and toluene indicates that regional transport across the Yellow Sea can be more important for longer-lived VOCs, while toluene remains more strongly controlled by local and domestic emissions.

NASA DC-8 observations provided broader regional and vertical context for the 1900D-based interpretation. The DC-8 chemical phase space distributions showed that Yellow Sea observations occupied a broad portion of the distribution and extended toward higher CO/CO_2 conditions, whereas Seoul observations were more concentrated in lower O_3/NO_x conditions. Within this chemical space, benzene enhancements extended toward higher CO/CO_2 conditions and were observed across a broader range of conditions, while toluene enhancements were more closely associated with fresher source-influenced conditions. These complementary observations support the interpretation that benzene retained a larger regional transport component, whereas toluene was more sensitive to localized source influences. Overall, the ASIA-AQ 1900D observations show that wintertime VOC distributions over the SMA and Yellow Sea were shaped jointly by chemical lifetime, emission source specificity, and regional

https://doi.org/10.5194/egusphere-2026-6595
Preprint. Discussion started: 10 November 2026
© Author(s) 2026. CC BY 4.0 License.

transport. The results highlight the importance of low-altitude airborne observations for resolving spatially heterogeneous VOC source influences in megacity environments. For wintertime VOC management in Seoul, domestic urban and industrial aromatic emissions remain central for reactive VOCs such as toluene and C_8 aromatics, while longer-lived compounds such as benzene require consideration of both local emissions and regional transport across the Yellow Sea.

Data availability

The Beechcraft 1900D observational data used in this study, including the PTR-ToF-MS and AIMMS-30 meteorological measurements, are available from the ASIA-AQ campaign archive (https://www-air.larc.nasa.gov/cgi-bin/ArcView/asiaaq; last access: 12 September 2026). The NASA DC-8 observations used in this study are publicly available at https://doi.org/10.5067/SUBORBITAL/ASIA-AQ/DATA001 (ASIA-AQ Science Team, 2025). The HYSPLIT model is available at https://www.ready.noaa.gov/HYSPLIT.php (last access: 12 September 2026).

Author contributions

JL curated the data, performed the formal analysis, and prepared the original draft and subsequent manuscript revisions. GL and ML conceptualized the study and established the analytical framework. GL contributed to the original draft, and ML substantially revised and finalized the manuscript. Jeongho Kim conducted airborne measurements and contributed to data acquisition. JP, LC, JC, MS, and Jongho Kim coordinated the 1900D airborne campaign and contributed to project administration and resources. Jeonghwan Kim contributed to manuscript review and editing. ECA, RSH, AF, CC, AW, WW, FP, DRB, IJS, SK, GSD, JAM, JPD, and YC contributed to the NASA DC-8 observations through measurement, processing, quality control, and provision of their respective VOC and supporting trace-gas datasets. IJS and RSH additionally provided detailed critical comments on the VOC analyses and scientific interpretation that substantially improved the manuscript. All authors discussed the results, reviewed the manuscript, and approved the final version.

Competing interests

The authors declare that they have no conflict of interest.

Acknowledgements

The authors gratefully acknowledge the ASIA-AQ science team for their efforts in planning and supporting the field campaign. The authors thank the NASA DC-8 flight and ground crews and instrument teams for their support of the airborne observations. The authors also thank the NIER airborne measurement team and the Hanseo University flight and ground crews for their support of the Beechcraft 1900D observations. IONICON Analytik is acknowledged for supplying a FUSION PTR-ToF-MS analyzer and providing staff support. OpenAI's ChatGPT

https://doi.org/10.5194/egusphere-2026-6595
Preprint. Discussion started: 10 November 2026
© Author(s) 2026. CC BY 4.0 License.

was used for language editing, wording refinement. All AI-assisted changes were reviewed and verified by the authors.

Financial support

This work was supported by the National Institute of Environmental Research (NIER), funded by the Ministry of Climate, Energy and Environment (MCEE) of the Republic of Korea (NIER-2024-01-01-005). This research was supported by the Korea Environmental Industry & Technology Institute (KEITI) through 2026 funding from the MCEE (No. RS-2026-25501457). This material is based upon work supported by the NSF National Center for Atmospheric Research, which is a major facility sponsored by the U.S. National Science Foundation under Cooperative Agreement No. 1852977. RSH and ECA were supported in part by NASA Award No. 80NSSC23K0818. PTR-ToF-MS measurements aboard the NASA DC-8 during ASIA-AQ were partially funded by the Austrian Federal Ministry for Climate Action, Environment, Energy, Mobility, Innovation, and Technology (BMK), represented by the Austrian Research Promotion Agency (FFG), through the Austrian Space Applications Programme (ASAP 2022, grant no. FO999900547). WW gratefully acknowledges the support from Gdańsk University of Technology through the DEC-4/1/2024/IDUB/II.1b/Am grant under the Americium International Career Development – "Excellence Initiative – Research University" program.

References

ASIA-AQ Science Team: Airborne and Satellite Investigation of Asian Air Quality Campaign Data, NASA Langley Atmospheric Science Data Center Distributed Active Archive Center [data set], https://doi.org/10.5067/SUBORBITAL/ASIA-AQ/DATA001, 2025.

Atkinson, R.: Gas-Phase Tropospheric Chemistry of Volatile Organic Compounds: 1. Alkanes and Alkenes, J. Phys. Chem. Ref. Data, 26, 215–290, https://doi.org/10.1063/1.556012, 1997.

Atkinson, R.: Atmospheric chemistry of VOCs and NO_x, Atmos. Environ., 34, 2063–2101, https://doi.org/10.1016/S1352-2310(99)00460-4, 2000.

Baek, S. O., Seo, Y. K., and Kim, J. H.: Occurrence and Distributions of Volatile Organic Compounds in the Ambient Air of Large Petro-chemical Industrial Complexes: Focusing on Daesan Area, J. Korean Soc. Atmos. Environ., 36, 32–47, https://doi.org/10.5572/KOSAE.2020.36.1.032, 2020.

Berkes, F., Hoor, P., Bozem, H., Kunkel, D., Sprenger, M., and Henne, S.: Airborne observation of mixing across the entrainment zone during PARADE 2011, Atmos. Chem. Phys., 16, 6011–6025, https://doi.org/10.5194/acp-16-6011-2016, 2016.

Blake, R. S., Monks, P. S., and Ellis, A. M.: Proton-transfer reaction mass spectrometry, Chem. Rev., 109, 861–896, https://doi.org/10.1021/cr800364q, 2009.

Caicedo, V., Rappenglueck, B., Cuchiara, G., Flynn, J., Ferrare, R., Scarino, A. J., Berkoff, T., Senff, C., Langford, A., and Lefer, B.: Bay Breeze and Sea Breeze Circulation Impacts on the Planetary Boundary Layer and Air Quality From an Observed and Modeled DISCOVER-AQ Texas Case Study, J. Geophys. Res.-Atmos., 124, 7359–7378, https://doi.org/10.1029/2019JD030523, 2019.

https://doi.org/10.5194/egusphere-2026-6595
Preprint. Discussion started: 10 November 2026
© Author(s) 2026. CC BY 4.0 License.



Cetin, E., Odabasi, M., and Seyfioglu, R.: Ambient volatile organic compound (VOC) concentrations around a petrochemical complex and a petroleum refinery, Sci. Total Environ., 312, 103–112, https://doi.org/10.1016/S0048-9697(03)00197-9, 2003.

Chen, X., Millet, D. B., Singh, H. B., Wisthaler, A., Apel, E. C., Atlas, E. L., Blake, D. R., Bourgeois, I., Brown, S. S., Crounse, J. D., de Gouw, J. A., Flocke, F. M., Fried, A., Heikes, B. G., Hornbrook, R. S., Mikoviny, T., Min, K. E., Müller, M., Neuman, J. A., O'sullivan, D. W., Peischl, J., Pfister, G. G., Richter, D., Roberts, J. M., Ryerson, T. B., Shertz, S. R., Thompson, C. R., Treadaway, V., Veres, P. R., Walega, J., Warneke, C., Washenfelder, R. A., Weibring, P., and Yuan, B.: On the sources and sinks of atmospheric VOCs: an integrated analysis of recent aircraft campaigns over North America, Atmos. Chem. Phys., 19, 9097–9123, https://doi.org/10.5194/acp-19-9097-2019, 2019.

Choi, J., Park, R. J., Lee, H. M., Lee, S., Jo, D. S., Jeong, J. I., Henze, D. K., Woo, J. H., Ban, S. J., Lee, M. D., Lim, C. S., Park, M. K., Shin, H. J., Cho, S., Peterson, D., and Song, C. K.: Impacts of local vs. trans-boundary emissions from different sectors on $PM_{2.5}$ exposure in South Korea during the KORUS-AQ campaign, Atmos. Environ., 203, 196–205, https://doi.org/10.1016/j.atmosenv.2019.02.008, 2019.

Choi, S.-W., Cho, H., Hong, Y., Jo, H.-J., Park, M., Lee, H.-J., Choi, Y.-J., Shin, H.-H., Lee, D., Shin, E., Baek, W., Park, S.-K., Kim, E., Kim, H.-C., Song, S.-J., Park, Y., Kim, J., Baek, J., Kim, J., and Yoo, C.: Analysis of the National Air Pollutant Emissions Inventory (CAPSS 2018) Data and Assessment of Emissions Based on Air Quality Modeling in the Republic of Korea, Asian J. Atmos. Environ., 16, 2022084, https://doi.org/10.5572/AJAE.2022.084, 2022.

Chun, H., Song, J., Park, J., Choi, W., Lee, K., and Song, M. Y.: Characteristics of the VOCs emitted from automotive painting workshop and control facilities, J. Odor Indoor Environ., 20, 39–50, https://doi.org/10.15250/JOIE.2021.20.1.39, 2021.

Crawford, J. H., Ahn, J. Y., Al-Saadi, J., Chang, L., Emmons, L. K., Kim, J., Lee, G., Park, J. H., Park, R. J., Woo, J. H., Song, C. K., Hong, J. H., Hong, Y. D., Lefer, B. L., Lee, M., Lee, T., Kim, S., Min, K. E., Yum, S. S., Shin, H. J., Kim, Y. W., Choi, J. S., Park, J. S., Szykman, J. J., Long, R. W., Jordan, C. E., Simpson, I. J., Fried, A., Dibb, J. E., Cho, S. Y., and Kim, Y. P.: The Korea-United States air quality (KORUS-AQ) field study, Elementa: Sci. Anthrop., 9, 00163, https://doi.org/10.1525/elementa.2020.00163, 2021.

Crawford, J. H., Travis, K. R., Judd, L. M., Lefer, B. L., Dibb, J. E., Kim, J., Park, R., Lee, G., Chang, L., Simpas, J. B. B., Cambaliza, M. O. L., MacAtangay, R. C., Surapipith, V., Thongboonchoo, N., Kim Oanh, N. T., Hien, T. T., Ly, B. T., Salam, A., Ghude, S. D., Latif, M. T., Yu, L. E., Tanimoto, H., and Kanaya, Y.: The Airborne and Satellite Investigation of Asian Air Quality (ASIA-AQ): An Opportunity for International Collaboration, International Geoscience and Remote Sensing Symposium (IGARSS), 6506–6509, https://doi.org/10.1109/IGARSS46834.2022.9883819, 2022.

de Gouw, J. and Warneke, C.: Measurements of volatile organic compounds in the earth's atmosphere using proton-transfer-reaction mass spectrometry, Mass Spectrom. Rev., 26, 223–257, https://doi.org/10.1002/mas.20119, 2007.

Derwent, R. G., Davies, T. J., Delaney, M., Dollard, G. J., Field, R. A., Dumitrean, P., Nason, P. D., Jones, B. M. R., and Pepler, S. A.: Analysis and interpretation of the continuous hourly monitoring data for 26 C_2–C_8 hydrocarbons at 12 United Kingdom sites during 1996, Atmos. Environ., 34, 297–312, https://doi.org/10.1016/S1352-2310(99)00203-4, 2000.

https://doi.org/10.5194/egusphere-2026-6595
Preprint. Discussion started: 10 November 2026
© Author(s) 2026. CC BY 4.0 License.

Fried, A., Walega, J., Weibring, P., Richter, D., Simpson, I. J., Blake, D. R., Blake, N. J., Meinardi, S., Barletta, B., Hughes, S. C., Crawford, J. H., Diskin, G., Barrick, J., Hair, J., Fenn, M., Wisthaler, A., Mikoviny, T., Woo, J.-H., Park, M., Kim, J., Min, K.-E., Jeong, S., Wennberg, P. O., Kim, M. J., Crounse, J. D., Teng, A. P., Bennett, R., Yang-Martin, M., Shook, M. A., Huey, G., Tanner, D., Knote, C., Kim, J., Park, R., and Brune, W.: Airborne formaldehyde and volatile organic compound measurements over the Daesan petrochemical complex on Korea's northwest coast during the Korea-United States Air Quality study: Estimation of emission fluxes and effects on air quality, Elementa: Sci. Anthrop., 8, 121, https://doi.org/10.1525/elementa.2020.121, 2020.

Gilman, J. B., Lerner, B. M., Kuster, W. C., Goldan, P. D., Warneke, C., Veres, P. R., Roberts, J. M., de Gouw, J. A., Burling, I. R., and Yokelson, R. J.: Biomass burning emissions and potential air quality impacts of volatile organic compounds and other trace gases from fuels common in the US, Atmos. Chem. Phys., 15, 13915–13938, https://doi.org/10.5194/acp-15-13915-2015, 2015.

Griffith, S. M., Huang, W. S., Lin, C. C., Chen, Y. C., Chang, K. E., Lin, T. H., Wang, S. H., and Lin, N. H.: Long-range air pollution transport in East Asia during the first week of the COVID-19 lockdown in China, Sci. Total Environ., 741, 140214, https://doi.org/10.1016/j.scitotenv.2020.140214, 2020.

Guenther, A., Massoli, P., Schaefer, K., and Tagaris, E.: Biological and Chemical Diversity of Biogenic Volatile Organic Emissions into the Atmosphere, Int. Sch. Res. Notices, 2013, 786290, https://doi.org/10.1155/2013/786290, 2013.

Guo, H., Wang, T., Blake, D. R., Simpson, I. J., Kwok, Y. H., and Li, Y. S.: Regional and local contributions to ambient non-methane volatile organic compounds at a polluted rural/coastal site in Pearl River Delta, China, Atmos. Environ., 40, 2345–2359, https://doi.org/10.1016/j.atmosenv.2005.12.011, 2006.

Hewitt, C. N., Hayward, S., and Tani, A.: The application of proton transfer reaction-mass spectrometry (PTR-MS) to the monitoring and analysis of volatile organic compounds in the atmosphere, J. Environ. Monit., 5, 1–7, https://doi.org/10.1039/b204712h, 2003.

Hudman, R. C., Murray, L. T., Jacob, D. J., Turquety, S., Wu, S., Millet, D. B., Avery, M., Goldstein, A. H., and Holloway, J.: North American influence on tropospheric ozone and the effects of recent emission reductions: Constraints from ICARTT observations, J. Geophys. Res.-Atmos., 114, D07302, https://doi.org/10.1029/2008JD010126, 2009.

Huebert, B. J., Bates, T., Russell, P. B., Shi, G., Kim, Y. J., Kawamura, K., Carmichael, G., and Nakajima, T.: An overview of ACE-Asia: Strategies for quantifying the relationships between Asian aerosols and their climatic impacts, J. Geophys. Res.-Atmos., 108, 8633, https://doi.org/10.1029/2003JD003550, 2003.

Itahashi, S., Uno, I., Osada, K., Kamiguchi, Y., Yamamoto, S., Tamura, K., Wang, Z., Kurosaki, Y., and Kanaya, Y.: Nitrate transboundary heavy pollution over East Asia in winter, Atmos. Chem. Phys., 17, 3823–3843, https://doi.org/10.5194/acp-17-3823-2017, 2017.

Jin, L., Permar, W., Selimovic, V., Ketcherside, D., Yokelson, R. J., Hornbrook, R. S., Apel, E. C., Ku, I. T., Collett, J. L., Sullivan, A. P., Jaffe, D. A., Pierce, J. R., Fried, A., Coggon, M. M., Gkatzelis, G. I., Warneke, C., Fischer, E. V., and Hu, L.: Constraining emissions of volatile organic compounds from western US wildfires with WE-CAN and FIREX-AQ airborne observations, Atmos. Chem. Phys., 23, 5969–5991, https://doi.org/10.5194/acp-23-5969-2023, 2023.

Kanaya, Y., Cao, R., Akimoto, H., Fukuda, M., Komazaki, Y., Yokouchi, Y., Koike, M., Tanimoto, H., Takegawa, N., and Kondo, Y.: Urban photochemistry in central Tokyo: 1. Observed and modeled OH and HO_2 radical

https://doi.org/10.5194/egusphere-2026-6595
Preprint. Discussion started: 10 November 2026
© Author(s) 2026. CC BY 4.0 License.

concentrations during the winter and summer of 2004, J. Geophys. Res.-Atmos., 112, D21312, https://doi.org/10.1029/2007JD008670, 2007.

Kim, C. H., Lee, H. J., Kang, J. E., Jo, H. Y., Park, S. Y., Jo, Y. J., Lee, J. J., Yang, G. H., Park, T., and Lee, T.: Meteorological Overview and Signatures of Long-range Transport Processes during the MAPS-Seoul 2015 Campaign, Aerosol Air Qual. Res., 18, 2173–2184, https://doi.org/10.4209/aaqr.2017.10.0398, 2018.

Kim, H., Park, R. J., Jeong, J. I., Choi, E., Woo, J. H., Kim, J., Song, C. H., Yu, J., Han, K. M., Song, C. K., Cha, Y., Lee, H. J., Kim, C. H., Baek, S. H., Kim, S., Jeong, S., Kim, E., Lee, M., Chang, L. S., and Crawford, J. H.: Ensemble-Based Source Attribution of Fine Particulate Matter over South Korea during the ASIA-AQ/SIJAQ Campaign, Environ. Sci. Technol., 60, 12292–12303, https://doi.org/10.1021/acs.est.5c15003, 2026.

Kim, J., Lee, G., Jun, J., Seo, B. K., and Choi, Y.: Quantification of SO_2 and CO_2 emission rates from coal-fired power plants in the Korean peninsula via airborne measurements, Sci. Total Environ., 978, 179430, https://doi.org/10.1016/j.scitotenv.2025.179430, 2025.

Kim, M. J., Seo, Y. K., Kim, J. H., and Baek, S. O.: Impact of industrial activities on atmospheric volatile organic compounds in Sihwa–Banwol, the largest industrial area in South Korea, Environ. Sci. Pollut. Res., 27, 28912–28930, https://doi.org/10.1007/s11356-020-09217-x, 2020.

Kim, S. Y.: A study on distribution characteristics of volatile organic compounds in Paju industrial complex area, using proton transfer reaction-time of flight mass spectrometry, Asian J. Atmos. Environ., 18, 2, https://doi.org/10.1007/s44273-023-00023-8, 2024.

Kleindienst, T. E., Smith, D. F., Li, W., Edney, E. O., Driscoll, D. J., Speer, R. E., and Weathers, W. S.: Secondary organic aerosol formation from the oxidation of aromatic hydrocarbons in the presence of dry submicron ammonium sulfate aerosol, Atmos. Environ., 33, 3669–3681, https://doi.org/10.1016/S1352-2310(99)00121-1, 1999.

Kwon, H. A., Park, R. J., Oak, Y. J., Nowlan, C. R., Janz, S. J., Kowalewski, M. G., Fried, A., Walega, J., Bates, K. H., Choi, J., Blake, D. R., Wisthaler, A., and Woo, J. H.: Top-down estimates of anthropogenic VOC emissions in South Korea using formaldehyde vertical column densities from aircraft during the KORUS-AQ campaign, Elementa: Sci. Anthrop., 9, 00109, https://doi.org/10.1525/elementa.2021.00109, 2021.

Lee, D., Kim, D., Lee, D., Song, M. Y., Kim, J. B., Choi, W., Hong, C. S., and Kim, K.: A Study on Distribution of Volatile Organic Compounds Concentration over Paju National Publishing Complex, J. Korean Soc. Atmos. Environ., 38, 599–609, https://doi.org/10.5572/KOSAE.2022.38.4.599, 2022.

Lee, J., Lee, M., Chang, L., Shin, S. A., Kim, K., Choi, Y., Lim, H., Choi, S. D., and Lee, G.: Assessment of VOCs emission inventory in Seoul through spatiotemporal observations using passive and online PAMS measurements, Atmos. Environ., 338, 120857, https://doi.org/10.1016/j.atmosenv.2024.120857, 2024.

Lee, K., Kim, Y. J., Kang, C. H., Kim, J. S., Chang, L. S., and Park, K.: Chemical characteristics of long-range-transported fine particulate matter at Gosan, Jeju island, in the spring and fall of 2008, 2009, 2011, and 2012, J. Air Waste Manage. Assoc., 65, 445–454, https://doi.org/10.1080/10962247.2014.1001883, 2015.

Li, Y., Barth, M. C., Chen, G., Patton, E. G., Kim, S. W., Wisthaler, A., Mikoviny, T., Fried, A., Clark, R., and Steiner, A. L.: Large-eddy simulation of biogenic VOC chemistry during the DISCOVER-AQ 2011 campaign, J. Geophys. Res.-Atmos., 121, 8083–8105, https://doi.org/10.1002/2016JD024942, 2016.

Mazzuca, G. M., Ren, X., Loughner, C. P., Estes, M., Crawford, J. H., Pickering, K. E., Weinheimer, A. J., and Dickerson, R. R.: Ozone production and its sensitivity to NO_x and VOCs: Results from the DISCOVER-AQ field

https://doi.org/10.5194/egusphere-2026-6595
Preprint. Discussion started: 10 November 2026
© Author(s) 2026. CC BY 4.0 License.

experiment, Houston 2013, Atmos. Chem. Phys., 16, 14463–14474, https://doi.org/10.5194/acp-16-14463-2016, 2016.

Morgan, W. T., Allan, J. D., Bower, K. N., Highwood, E. J., Liu, D., McMeeking, G. R., Northway, M. J., Williams, P. I., Krejci, R., and Coe, H.: Airborne measurements of the spatial distribution of aerosol chemical composition across Europe and evolution of the organic fraction, Atmos. Chem. Phys., 10, 4065–4083, https://doi.org/10.5194/acp-10-4065-2010, 2010.

Müller, M., Mikoviny, T., Feil, S., Haidacher, S., Hanel, G., Hartungen, E., Jordan, A., Märk, L., Mutschlechner, P., Schottkowsky, R., Sulzer, P., Crawford, J. H., and Wisthaler, A.: A compact PTR-ToF-MS instrument for airborne measurements of volatile organic compounds at high spatiotemporal resolution, Atmos. Meas. Tech., 7, 3763–3772, https://doi.org/10.5194/amt-7-3763-2014, 2014.

National Institute of Environmental Research (NIER): Annual Report of Air Quality in Korea 2023, NIER-GP 2024-050, National Institute of Environmental Research, Incheon, Republic of Korea, 407 pp., https://www.airkorea.or.kr (last access: 29 June 2026), 2024.

Nault, B. A., Campuzano-Jost, P., Day, D. A., Schroder, J. C., Anderson, B., Beyersdorf, A. J., Blake, D. R., Brune, W. H., Choi, Y., Corr, C. A., de Gouw, J. A., Dibb, J., DiGangi, J. P., Diskin, G. S., Fried, A., Huey, L. G., Kim, M. J., Knote, C. J., Lamb, K. D., Lee, T., Park, T., Pusede, S. E., Scheuer, E., Thornhill, K. L., Woo, J. H., and Jimenez, J. L.: Secondary organic aerosol production from local emissions dominates the organic aerosol budget over Seoul, South Korea, during KORUS-AQ, Atmos. Chem. Phys., 18, 17769–17800, https://doi.org/10.5194/acp-18-17769-2018, 2018.

Park, H. Y., Ahn, J. Y., Hong, S. C., Lee, J. B., and Cho, S. Y.: The formation and transport of HNO_3 over the Yellow Sea and its impact on the January 2018 $PM_{2.5}$ episode in Seoul, Environ. Sci.-Atmos., 4, 670–684, https://doi.org/10.1039/d4ea00034j, 2024.

Park, J. M., Park, J. Y., and Park, H. S.: A review of the National Eco-Industrial Park Development Program in Korea: progress and achievements in the first phase, 2005–2010, J. Clean. Prod., 114, 33–44, https://doi.org/10.1016/j.jclepro.2015.08.115, 2016.

Park, S. S., Kim, Y. J., and Fung, K.: Characteristics of $PM_{2.5}$ carbonaceous aerosol in the Sihwa industrial area, Korea, Atmos. Environ., 35, 657–665, https://doi.org/10.1016/S1352-2310(00)00357-5, 2001.

Parrish, D. D., Stohl, A., Forster, C., Atlas, E. L., Blake, D. R., Goldan, P. D., Kuster, W. C., and de Gouw, J. A.: Effects of mixing on evolution of hydrocarbon ratios in the troposphere, J. Geophys. Res.-Atmos., 112, D10S34, https://doi.org/10.1029/2006JD007583, 2007.

Piel, F., Müller, M., Mikoviny, T., Pusede, S. E., and Wisthaler, A.: Airborne measurements of particulate organic matter by proton-transfer-reaction mass spectrometry (PTR-MS): A pilot study, Atmos. Meas. Tech., 12, 5947–5958, https://doi.org/10.5194/amt-12-5947-2019, 2019.

Ren, X., Brune, W. H., Mao, J., Mitchell, M. J., Lesher, R. L., Simpas, J. B., Metcalf, A. R., Schwab, J. J., Cai, C., Li, Y., Demerjian, K. L., Felton, H. D., Boynton, G., Adams, A., Perry, J., He, Y., Zhou, X., and Hou, J.: Behavior of OH and HO_2 in the winter atmosphere in New York City, Atmos. Environ., 40, 252–263, https://doi.org/10.1016/j.atmosenv.2005.11.073, 2006.

Ryerson, T. B., Andrews, A. E., Angevine, W. M., Bates, T. S., Brock, C. A., Cairns, B., Cohen, R. C., Cooper, O. R., de Gouw, J. A., Fehsenfeld, F. C., Ferrare, R. A., Fischer, M. L., Flagan, R. C., Goldstein, A. H., Hair, J. W., Hardesty, R. M., Hostetler, C. A., Jimenez, J. L., Langford, A. O., McCauley, E., McKeen, S. A., Molina, L.

https://doi.org/10.5194/egusphere-2026-6595
Preprint. Discussion started: 10 November 2026
© Author(s) 2026. CC BY 4.0 License.



T., Nenes, A., Oltmans, S. J., Parrish, D. D., Pederson, J. R., Pierce, R. B., Prather, K., Quinn, P. K., Seinfeld, J. H., Senff, C. J., Sorooshian, A., Stutz, J., Surratt, J. D., Trainer, M., Volkamer, R., Williams, E. J., and Wofsy, S. C.: The 2010 California Research at the Nexus of Air Quality and Climate Change (CalNex) field study, J. Geophys. Res.-Atmos., 118, 5830–5866, https://doi.org/10.1002/jgrd.50331, 2013.

Ryerson, T. B., Trainer, M., Angevine, W. M., Brock, C. A., Dissly, R. W., Fehsenfeld, F. C., Frost, G. J., Goldan, P. D., Holloway, J. S., Hübler, G., Jakoubek, R. O., Kuster, W. C., Neuman, J. A., Nicks, D. K., Parrish, D. D., Roberts, J. M., Sueper, D. T., Atlas, E. L., Donnelly, S. G., Flocke, F., Fried, A., Potter, W. T., Schauffler, S., Stroud, V., Weinheimer, A. J., Wert, B. P., Wiedinmyer, C., Alvarez, R. J., Banta, R. M., Darby, L. S., and Senff, C. J.: Effect of petrochemical industrial emissions of reactive alkenes and NO_x on tropospheric ozone formation in Houston, Texas, J. Geophys. Res.-Atmos., 108, 4249, https://doi.org/10.1029/2002JD003070, 2003.

Sarkar, C., Wong, G., Mielnik, A., Nagalingam, S., Gross, N. J., Guenther, A. B., Lee, T., Park, T., Ban, J., Kang, S., Park, J. S., Ahn, J., Kim, D., Kim, H., Choi, J., Seo, B. K., Kim, J. H., Kim, J. H., Park, S. B., and Kim, S.: Unexplored volatile organic compound emitted from petrochemical facilities: Implications for ozone production and atmospheric chemistry, Atmos. Chem. Phys., 21, 11505–11518, https://doi.org/10.5194/acp-21-11505-2021, 2021.

Sasakawa, M., Machida, T., Tsuda, N., Arshinov, M., Davydov, D., Fofonov, A., and Krasnov, O.: Aircraft and tower measurements of CO_2 concentration in the planetary boundary layer and the lower free troposphere over southern taiga in West Siberia: Long-term records from 2002 to 2011, J. Geophys. Res.-Atmos., 118, 9489–9498, https://doi.org/10.1002/jgrd.50755, 2013.

Seidel, D. J., Ao, C. O., and Li, K.: Estimating climatological planetary boundary layer heights from radiosonde observations: Comparison of methods and uncertainty analysis, J. Geophys. Res.-Atmos., 115, D16113, https://doi.org/10.1029/2009JD013680, 2010.

Seinfeld, J. H. and Pandis, S. N.: Atmospheric Chemistry and Physics: From Air Pollution to Climate Change, 3rd Edn., John Wiley & Sons, Hoboken, NJ, USA, 1152 pp., ISBN 978-1-118-94740-1, 2016.

Shin, S.-H., Park, J.-S., Kim, J. B., Kim, P., Kim, C. H., Hwang, K., Park, S.-M., Lee, J., Park, J.-M., and Kim, J.: Characteristics of Volatile Organic Compounds Distribution in Downtown Ansan Near Industrial Complexes, J. Environ. Anal. Health Toxicol., 27, 14–28, https://doi.org/10.36278/JEAHT.27.1.14, 2024.

Simpson, I. J., Blake, D. R., Blake, N. J., Meinardi, S., Barletta, B., Hughes, S. C., Fleming, L. T., Crawford, J. H., Diskin, G. S., Emmons, L. K., Fried, A., Guo, H., Peterson, D. A., Wisthaler, A., Woo, J.-H., Barré, J., Gaubert, B., Kim, J., Kim, M. J., Kim, Y., Knote, C., Mikoviny, T., Pusede, S. E., Schroeder, J. R., Wang, Y., Wennberg, P. O., and Zeng, L.: Characterization, sources and reactivity of volatile organic compounds (VOCs) in Seoul and surrounding regions during KORUS-AQ, Elementa: Sci. Anthrop., 8, 37, https://doi.org/10.1525/elementa.434, 2020.

Singh, H. B., Salas, L. J., Chatfield, R. B., Czech, E., Fried, A., Walega, J., Evans, M. J., Field, B. D., Jacob, D. J., Blake, D., Heikes, B., Talbot, R., Sachse, G., Crawford, J. H., Avery, M. A., Sandholm, S., and Fuelberg, H.: Analysis of the atmospheric distribution, sources, and sinks of oxygenated volatile organic chemicals based on measurements over the Pacific during TRACE-P, J. Geophys. Res.-Atmos., 109, D15S07, https://doi.org/10.1029/2003JD003883, 2004.

Stone, D., Whalley, L. K., and Heard, D. E.: Tropospheric OH and HO_2 radicals: field measurements and model comparisons, Chem. Soc. Rev., 41, 6348–6404, https://doi.org/10.1039/c2cs35140d, 2012.

https://doi.org/10.5194/egusphere-2026-6595
Preprint. Discussion started: 10 November 2026
© Author(s) 2026. CC BY 4.0 License.



Travis, K. R., Heald, C. L., Allen, H. M., Apel, E. C., Arnold, S. R., Blake, D. R., Brune, W. H., Chen, X., Commane, R., Crounse, J. D., Daube, B. C., Diskin, G. S., Elkins, J. W., Evans, M. J., Hall, S. R., Hintsa, E. J., Hornbrook, R. S., Kasibhatla, P. S., Kim, M. J., Luo, G., McKain, K., Millet, D. B., Moore, F. L., Peischl, J., Ryerson, T. B., Sherwen, T., Thames, A. B., Ullmann, K., Wang, X., Wennberg, P. O., Wolfe, G. M., and Yu, F.: Constraining remote oxidation capacity with ATom observations, Atmos. Chem. Phys., 20, 7753–7781, https://doi.org/10.5194/acp-20-7753-2020, 2020.

Wang, S., Li, Q., Duan, K., Wang, B., Zhu, X., Wang, X., Shen, Y., Liu, H., and Ma, Y.: Profile of atmospheric VOC over the Yellow Sea, China: A tale of distribution, constraints, and sources, Sci. Total Environ., 868, 161634, https://doi.org/10.1016/j.scitotenv.2023.161634, 2023.

Warneke, C., de Gouw, J. A., Edwards, P. M., Holloway, J. S., Gilman, J. B., Kuster, W. C., Graus, M., Atlas, E., Blake, D., Gentner, D. R., Goldstein, A. H., Harley, R. A., Alvarez, S., Rappenglueck, B., Trainer, M., and Parrish, D. D.: Photochemical aging of volatile organic compounds in the Los Angeles basin: Weekday-weekend effect, J. Geophys. Res.-Atmos., 118, 5018–5028, https://doi.org/10.1002/jgrd.50423, 2013.

Wu, Y. C., Li, J. L., Wang, J., Zhuang, G. C., Liu, X. T., Zhang, H. H., and Yang, G. P.: Occurance, emission and environmental effects of non-methane hydrocarbons in the Yellow Sea and the East China Sea, Environ. Pollut., 270, 116305, https://doi.org/10.1016/j.envpol.2020.116305, 2021.

Yuan, B., Shao, M., Lu, S., and Wang, B.: Source profiles of volatile organic compounds associated with solvent use in Beijing, China, Atmos. Environ., 44, 1919–1926, https://doi.org/10.1016/j.atmosenv.2010.02.014, 2010.